

Medium- and high-spin band structure of the chiral-candidate nucleus ^{134}Pr

J. Timár,¹ K. Starosta,^{2,3} I. Kuti,¹ D. Sohler,¹ D. B. Fossan,² T. Koike,^{2,4} E. S. Paul,⁵ A. J. Boston,⁵ H. J. Chantler,⁵ M. Descovich,⁵ R. M. Clark,⁶ M. Cromaz,⁶ P. Fallon,⁶ I. Y. Lee,⁶ A. O. Macchiavelli,⁶ C. J. Chiara,^{2,7,8} R. Wadsworth,⁹ A. A. Hecht,¹⁰ D. Almeded,¹¹ and S. Frauendorf¹¹

¹*Institute of Nuclear Research, Pf. 51, HU-4001 Debrecen, Hungary*

²*Department of Physics and Astronomy, State University of New York at Stony Brook, Stony Brook, New York 11794-3800, USA*

³*Department of Chemistry, Simon Fraser University, Burnaby, British Columbia V5A 1S6, Canada*

⁴*Graduate School of Science, Tohoku University, Sendai, 980-8578, Japan*

⁵*Oliver Lodge Laboratory, Department of Physics, University of Liverpool, Liverpool L69 7ZE, UK*

⁶*Nuclear Science Division, Lawrence Berkeley National Laboratory, Berkeley, California 94720, USA*

⁷*Department of Chemistry and Biochemistry, University of Maryland, College Park, Maryland 20742, USA*

⁸*Physics Division, Argonne National Laboratory, Argonne, Illinois 60439, USA*

⁹*Department of Physics, University of York, York YO10 5DD, UK*

¹⁰*Wright Nuclear Structure Laboratory, Yale University, New Haven, Connecticut 06520, USA*

¹¹*Physics Department, University of Notre Dame, Notre Dame, Indiana 46556, USA*

(Received 23 May 2011; published 5 October 2011)

Medium- and high-spin states of ^{134}Pr were populated using the $^{116}\text{Cd}(^{23}\text{Na}, 5n)$ reaction and studied with the GAMMASPHERE spectrometer. Several new bands have been found in this nucleus, one of them being linked to the previously observed chiral-candidate twin-band structure. The ground state of ^{134}Pr could be determined through establishing a level structure that connects the two previously known long-lived isomeric states. Unambiguous spin-parity assignments for the excited states could be performed based on the known 2^- spin-parity of the ground state combined with the present experimental data. Intrinsic single-particle configurations have been assigned to the newly observed bands on the basis of the measured $B(M1)/B(E2)$ ratios, alignments, band-crossing frequencies, bandhead spins, the observed single-particle configurations in the neighboring nuclei, and taking into account the predictions of total Routhian surface and tilted-axis cranking calculations.

DOI: [10.1103/PhysRevC.84.044302](https://doi.org/10.1103/PhysRevC.84.044302)

PACS number(s): 21.10.Hw, 21.10.Re, 21.60.-n, 23.20.Lv

I. INTRODUCTION

Unambiguous identification of intrinsic chirality in rotating triaxial nuclei is one of the most intriguing tasks of contemporary high-spin nuclear structure studies. Intrinsic chirality is generated when the total angular momentum vector of a rotating triaxial nucleus is out of the three symmetry planes of the triaxial mean field [1,2]. According to recent model calculations the experimental manifestation of this intrinsic chirality is a structure of two, almost degenerate, $\Delta I = 1$ rotational bands having equal parity and linked to each other by inter-band γ -ray transitions. Such rotational doublet-band candidates for chiral structures have been observed mostly in two regions of the nuclear chart: around ^{134}Pr (see, e.g., Refs. [3–16]) and around ^{104}Rh (see, e.g., Refs. [17–22]).

One of the key nuclei among the chiral candidates is ^{134}Pr . The strongly linked $\Delta I = 1$ rotational band structure, found by Petrache *et al.* [3] and assigned to the $\pi h_{11/2} \nu h_{11/2}$ configuration, was the first experimental candidate for chiral rotation [1]. Since the publication of the chiral hypothesis for ^{134}Pr , this nucleus has been a subject of many experimental and theoretical studies [4,9,15,23–27] providing several different scenarios for the nature of the chiral-candidate band structure. However, the many studies published up to now on ^{134}Pr concentrated mainly on the known chiral-candidate band structure in this nucleus, and thus, in many experimental

aspects, the level scheme of this nucleus cannot be considered well known.

High-spin rotational bands in this nucleus were reported by Beausang *et al.* [28], Petrache *et al.* [3], and Hauschild *et al.* [29]. Besides the chiral-candidate band structure, three additional rotational bands were reported. These include a negative-parity four-quasiparticle band, assigned the $\pi[413]5/2(h_{11/2})^2 \nu h_{11/2}$ configuration, in addition to two doubly decoupled bands, assigned to $\pi h_{11/2} \nu[530]1/2$ and $\pi h_{11/2} \nu[660]1/2$ configurations, respectively. The latter could not be linked to the rest of the level scheme and has a tentative parity assignment. The lifetimes of levels in the doubly decoupled bands were later measured by Rao *et al.* [30], while the lifetimes of the chiral-candidate band structure were reported by Tonev *et al.* [23].

No negative-parity two-quasiparticle bands have been reported in this nucleus, although they are expected. Also, the problem of deciding which of the two long-lived isomeric states is the ground state and which is the excited state has not been solved. Moreover, even for the known states and bands, the reported spins and parities are assigned tentatively. The aim of the present paper is to establish a more detailed level scheme of ^{134}Pr to enrich our knowledge of the active valence particles and the shape stability of this nucleus. This information is relevant also to studies addressing the chiral-candidate band structure.

II. EXPERIMENTAL METHODS AND RESULTS

Excited states in ^{134}Pr were populated following the $^{116}\text{Cd}(^{23}\text{Na}, 5n)$ reaction at a beam energy of 115 MeV. The experiment was performed at the Lawrence Berkeley National Laboratory, using a ^{23}Na beam supplied by the 88-inch cyclotron. The experimental setup consisted of the GAMMASPHERE spectrometer of 99 HPGe detectors in 16 rings covering a large fraction of the full solid angle [31,32] (with ring 1 at $\theta = 17.3^\circ$ being empty). In order to obtain γ -ray sum-energy and multiplicity information, the Hevimet collimators ordinarily placed in front of the BGO Compton-suppression shields were removed for this experiment as discussed in Ref. [33]. The sum-energy and multiplicity data were not used in the present analysis; however, they were important in studying other nuclei from this experiment [34].

The experiment consisted of two runs: Run 1 uses a 1.00 mg/cm² thick ^{116}Cd target backed with 15 mg/cm² ^{208}Pb aimed at performing lifetime measurements using the Doppler shift attenuation method (DSAM) [35], while Run 2 uses a self-supporting 1.22 mg/cm² thick ^{116}Cd target aimed to identify the high-spin states in ^{134}Pr . The current paper reports results from both runs; however, the DSAM analysis will be addressed in a separate paper.

For the off-line analysis, coincident γ rays were sorted using the BLUE and RADWARE software packages following the procedures defined in Refs. [36] and [37], respectively. The details of the data analysis with the BLUE package, especially the handling of background subtraction for the DSAM analysis, are addressed in Ref. [38]. The γ -ray energies observed in Run 2 were corrected for Doppler shifts. The average velocity of the recoiling nuclei was measured to be $\beta \sim 1.380(5)\%$, in agreement with the value calculated based on reaction kinematics. For Run 2 a γ -ray energy resolution of $\Delta E_\gamma \sim 3.8$ keV full width at half maximum (FWHM) at $E_\gamma \sim 660$ keV was achieved; the resolution was measured using the $19/2^- \rightarrow 15/2^-$ transition in ^{133}Pr .

An angular-correlation analysis, based on the directional correlation of oriented states (DCO) method [39] was performed for γ -ray multipolarity assignments. This analysis was carried out based on the spectra extracted from the BLUE database for the backed target Run 1 with the background subtracted according to the prescription of Ref. [38]. In the geometry used, R_{DCO} values of 1 and ~ 0.6 are expected for the stretched quadrupole ($\Delta I = 2$) and pure stretched dipole ($\Delta I = 1$) transitions, respectively, when gating on a quadrupole transition. Using a stretched dipole gate with minimal quadrupole mixing, the expected values are ~ 1.7 and ~ 1 , respectively. The expected R_{DCO} values for $\Delta I = 0$ dipole transitions are similar to the ones for the stretched quadrupole transitions.

In order to analyze the γ -ray coincidence relations and to build the level scheme of ^{134}Pr the collected events were sorted into RADWARE cubes separately for the thin-target data and the thick-target data. They contained approximately 7×10^9 and 9×10^9 triple coincidences, respectively. The good statistics of the experiment enabled us to assign a large number of new γ rays to ^{134}Pr and determine their multiplicities. Altogether

approximately 360 γ transitions have been assigned to this nucleus, more than half of them being identified for the first time in the present experiment. The properties of the observed ^{134}Pr γ rays are given in Table I. In the table, we accepted $E2$ multipolarity for all the γ rays with R_{DCO} values corresponding to quadrupole transitions. If the transition is a stretched dipole on the basis of its R_{DCO} value, we took into account other possible arguments in order to determine its electric and magnetic character. For example, for an in-band stretched dipole transition, we accepted $M1$ multipolarity. Example double-gated, background-subtracted coincidence spectra are plotted in Fig. 1.

III. LEVEL SCHEME

From the observed $\gamma\gamma\gamma$ -coincidence relations we have built a more complete level scheme of ^{134}Pr . The observed data also enabled us to determine which of the two long-lived isomeric states is the ground state of ^{134}Pr and to obtain unambiguous spin and parity assignments for the excited states of this nucleus, which were only tentatively known before the present experiment. The derived level scheme contains 13 bands, among which 9 are newly assigned to ^{134}Pr . For the sake of clarity the level scheme is plotted in Figs. 2, 3, and 4, respectively.

A. Low- and medium-spin negative-parity bands

Two long-lived isomeric states are known in ^{134}Pr . One has a 17-min lifetime and its spin-parity is unambiguously determined as 2^- from the β decay of ^{134}Nd [40]. The other has an 11-min lifetime and was observed in heavy-ion-induced reactions; however, its spin-parity could not be unambiguously determined. Possible 5^- , 7^- , and 6^- values have been suggested for its spin-parity in Refs. [41–43]. The energy difference between the two isomers was unknown up to the present experiment. Petrache *et al.* [3] observed the $M1$ cascade of band 12 and other γ transitions in coincidence with that cascade. They realized that this cascade feeds the 2^- isomeric state and that it is connected to band 5; however, they could not establish the corresponding level structure due to lack of statistics.

Five new negative-parity bands at low to medium spins (bands 9, 10, 11, 12, and 13 in Fig. 2) have been derived from the present experiment. Band 12 decays by the 332- and the 614-keV transitions to the state which is identified from the previous heavy-ion reaction studies as the 11-min isomeric state. However, the bandhead of band 12 lies 68 keV lower than this state, and this is the lowest-lying level in the observed level scheme. Therefore, it is straightforward to identify this bandhead as the 17-min isomeric state. Thus, these linking transitions fix the relative position of the two isomeric states, with the 17-min state being the ground state and the 11-min state having an excitation energy of 68 keV. The five bands shown in Fig. 2 are linked together through many γ transitions, and there are also several other paths that link the two isomeric states together, thus confirming the relative positions stated above.

TABLE I. Energies, relative intensities, DCO ratios, and multiplicities of γ rays assigned to ^{134}Pr in the present work, as well as the band assignment for the initial state, the spin-parities of the initial and final states, and the excitation energy of the initial state for the decay. The experimental errors of the relative intensities for the strong and/or well-resolved transitions are on the order of 5% while for weak or compound lines the errors can rise up to 50%. DCO ratios were determined using quadrupole gates if not indicated otherwise. l_s denotes the small level structure between bands 10 and 11. D denotes dipole transition.

E_γ (keV)	I_γ	R_{DCO}	Mult.	Band _{<i>i</i>}	$I_i^\pi \rightarrow I_f^\pi$	E_i (keV)
39.3(3)	21.5		$M1^a$	1	$8^+ \rightarrow 7^+$	414
46.5(4)	0.1			11	$7^- \rightarrow 6^-$	751
82.4(4)	0.4		$E1^b$	1	$7^+ \rightarrow 7^-$	374
90.7(3)	0.7			9	$7^- \rightarrow 7^-$	383
94.6(3)	39.2	0.74(5)	$M1^a$	1	$9^+ \rightarrow 8^+$	508
103.1(2)	0.2			9	$8^- \rightarrow 8^-$	653
109.3(3)	0.2			13	$8^- \rightarrow (7^-)$	906
115.7(2)	5.8	0.57(5)	$M1$	12	$3^- \rightarrow 2^-$	116
117.9(2)	3.8	0.58(5)	$M1$	12	$6^- \rightarrow 5^-$	517
120.7(3)	0.2			11	$6^- \rightarrow (6^-)$	705
121.9(3)	0.3		$E1^b$	1	$8^+ \rightarrow 7^-$	414
130.6(2)	4.4			11	$8^- \rightarrow 7^-$	882
131.3(2)	5.0	0.51(4)	$M1$	12	$4^- \rightarrow 3^-$	247
133.9(2)	0.6	0.43(13)	$M1$	3	$10^+ \rightarrow 9^+$	1306
146.3(2)	1.6	0.46(6)	D	5	$14^- \rightarrow 13^-$	2748
152.5(2)	5.2	0.56(5)	$M1$	12	$5^- \rightarrow 4^-$	400
164.5(2)	3.6	0.64(6)	$M1$	12	$7^- \rightarrow 6^-$	682
166.4(2)	1.1			2	$11^+ \rightarrow 10^+$	1304
166.9(3)	0.1			11	$7^- \rightarrow (6^-)$	751
167.5(4)	0.2			2	$9^+ \rightarrow 8^+$	933
171.2(2)	71.9	0.55(2)	$M1$	1	$10^+ \rightarrow 9^+$	679
171.3(3)	0.2			2	$10^+ \rightarrow 11^+$	1138
179.2(2)	0.8	1.59(24) ^c	D	11	$9^- \rightarrow 8^-$	1086
184.7(3)	0.7		l_s		$(6^-) \rightarrow 5^-$	584
187.3(3)	0.1			13	$10^- \rightarrow (9^-)$	1468
199.8(3)	0.5	0.93(27) ^c	$M1$	6	$14^- \rightarrow 13^-$	2910
200.6(2)	12.7	0.57(9)	$M1$	5	$14^- \rightarrow 13^-$	2748
204.0(3)	2.7	0.90(6) ^c	$M1$	11	$9^- \rightarrow 8^-$	1086
204.6(2)	17.3	0.63(7)	$M1$	5	$15^- \rightarrow 14^-$	2953
204.8(2)	0.8			2	$10^+ \rightarrow 9^+$	1138
210.7(2)	1.7	0.46(5)	$M1$	3	$11^+ \rightarrow 10^+$	1516
212.8(3)	0.2		l_s		$(7^-) \rightarrow (6^-)$	797
215.8(2)	0.7			10	$9^- \rightarrow 8^-$	869
216.3(2)	1.3			5	$12^- \rightarrow 11^-$	2317
224.3(2)	14.6			10	$7^- \rightarrow 6^-$	292
224.7(2)	1.0	0.53(10)	D	13	$8^- \rightarrow 7^-$	906
225.0(6)	0.6			12	$6^- \rightarrow 7^-$	517
227.5(2)	1.5	1.06(19) ^c	$M1$	6	$15^- \rightarrow 14^-$	3137
230.4(2)	4.2	0.32(13)	$M1$	5	$13^- \rightarrow 12^-$	2548
233.9(3)	1.3	0.79(8) ^c	D	11	$7^- \rightarrow 6^-$	751
239.6(3)	0.3			10	$11^- \rightarrow 10^-$	1573
240.0(2)	19.2			5	$16^- \rightarrow 15^-$	3193
243.3(2)	0.4	0.43(19)	D	3	$11^+ \rightarrow 12^+$	1516
245.0(2)	1.6	0.51(6)	D	4	$11^+ \rightarrow 10^+$	1551
246.6(4)	0.2			10	$13^- \rightarrow 12^-$	2380
250.2(2)	0.8			3	$13^+ \rightarrow 12^+$	2034
251.1(2)	2.9	0.37(8)	D	13	$9^- \rightarrow 8^-$	1133
253.4(4)	0.9			11	$10^- \rightarrow 9^-$	1386
253.6(4)	0.2			2	$9^+ \rightarrow 10^+$	933

TABLE I. (Continued.)

E_γ (keV)	I_γ	R_{DCO}	Mult.	Band _{<i>i</i>}	$I_i^\pi \rightarrow I_f^\pi$	E_i (keV)
257.1(3)	0.2			2	$8^+ \rightarrow 9^+$	765
257.8(2)	6.9	0.23(5)	$M1$	10	$8^- \rightarrow 7^-$	550
258.2(3)	0.2			7	$16^- \rightarrow 15^-$	3545
267.2(2)	0.6			3	$12^+ \rightarrow 11^+$	1784
270.0(2)	2.1			9	$8^- \rightarrow 7^-$	653
270.3(3)	0.4			12	$6^- \rightarrow 4^-$	517
277.6(2)	0.7	0.42(12)	D	4	$11^+ \rightarrow 12^+$	1551
280.0(2)	4.6	0.48(12)	$M1$	6	$16^- \rightarrow 15^-$	3417
283.3(2)	6.9	1.33(36) ^c	$M1$	2	$12^+ \rightarrow 11^+$	1587
283.9(4)	0.2			12	$5^- \rightarrow 3^-$	400
287.6(2)	62.7			1	$11^+ \rightarrow 10^+$	967
289.9(2)	20.0	0.65(8)	$M1$	5	$17^- \rightarrow 16^-$	3483
290.8(4)	1.3			5	$14^- \rightarrow 13^-$	2748
292.3(2)	1.1			7	$16^- \rightarrow 15^-$	3545
293.8(2)	1.9	1.10(18) ^c	D	6	$15^- \rightarrow 14^-$	3137
300.8(2)	2.3	0.30(4)	$M1$	11	$10^- \rightarrow 9^-$	1386
305.3(3)	1.0			11	$6^- \rightarrow 5^-$	705
306.5(3)	40.4			1	$12^+ \rightarrow 11^+$	1273
306.6(2)	100.0	0.58(4)	D	1	$7^+ \rightarrow 6^-$	374
307.6(3)	0.3			9	$10^- \rightarrow 9^-$	1333
315.0(2)	1.5	0.34(14)	D	9	$7^- \rightarrow 6^-$	383
316.5(2)	1.4			7	$17^- \rightarrow 16^-$	3861
318.8(2)	5.4			10	$9^- \rightarrow 8^-$	869
318.9(2)	5.0			6	$17^- \rightarrow 16^-$	3736
323.9(2)	14.6	0.49(7)	$M1$	2	$13^+ \rightarrow 12^+$	1911
324.4(3)	0.2			10	$15^- \rightarrow 14^-$	3286
331.8(3)	1.3	0.48(10)	D	12	$5^- \rightarrow 6^-$	400
332.1(5)	0.4			11	$8^- \rightarrow 8^-$	882
332.5(2)	1.6	0.53(11)	$M1$	11	$11^- \rightarrow 10^-$	1719
333.8(4)	0.4			10	$13^- \rightarrow 12^-$	2380
334.4(3)	0.4			11	$9^- \rightarrow 7^-$	1086
334.8(3)	0.4	1.11(38) ^c	$M1$	13	$10^- \rightarrow 9^-$	1468
337.1(2)	13.1	0.46(10)	$M1$	2	$14^+ \rightarrow 13^+$	2248
337.6(4)	1.0			11	$7^- \rightarrow 8^+$	751
339.2(2)	2.3	0.64(8)	D	3	$10^+ \rightarrow 11^+$	1306
339.8(2)	1.2	0.28(7)	$M1$	10	$11^- \rightarrow 10^-$	1573
339.8(2)	1.2	0.49(22)	$M1$	7	$18^- \rightarrow 17^-$	4201
343.0(2)	15.4	0.61(10)	$M1$	5	$18^- \rightarrow 17^-$	3826
358.1(2)	1.2			3	$14^+ \rightarrow 13^+$	2392
359.8(2)	4.0	0.95(17) ^c	$M1$	6	$18^- \rightarrow 17^-$	4096
364.1(2)	1.1			10	$10^- \rightarrow 9^-$	1233
364.5(3)	0.5			11	$8^- \rightarrow 6^-$	882
364.6(3)	0.2			4	$9^+ \rightarrow 8^+$	1130
368.3(2)	1.2	0.42(11)	D	5	$14^- \rightarrow 13^-$	2748
369.2(2)	6.1			2	$15^+ \rightarrow 14^+$	2617
372.8(3)	0.7			9	$9^- \rightarrow 8^-$	1026
376.9(4)	0.5			11	$7^- \rightarrow 7^+$	751
377.8(3)	0.3			4	$13^+ \rightarrow 12^+$	2161
378.5(3)	0.4	0.31(17)	$M1$	13	$12^- \rightarrow 11^-$	2158
381.7(3)	1.0			13	$9^- \rightarrow 7^-$	1133
382.1(3)	0.3			13	$10^- \rightarrow 9^-$	1468
382.5(3)	1.6	0.40(6)	$M1$	11	$12^- \rightarrow 11^-$	2101
386.1(2)	10.7	0.64(16)	$M1$	5	$19^- \rightarrow 18^-$	4212
386.5(4)	0.8	0.29(7)	$M1$	11	$14^- \rightarrow 13^-$	2844
389.4(4)	0.8	0.98(15)	$E2$	13	$8^- \rightarrow 6^-$	906
389.8(3)	1.2			5	$13^- \rightarrow 12^-$	2548
390.7(3)	0.1			2	$8^+ \rightarrow 7^+$	765
393.0(3)	1.2			13	$11^- \rightarrow 10^-$	1779

TABLE I. (*Continued.*)

E_γ (keV)	I_γ	R_{DCO}	Mult.	Band _{<i>i</i>}	$I_i^\pi \rightarrow I_f^\pi$	E_i (keV)
395.6(2)	13.8			1	14 ⁺ → 13 ⁺	2085
396.9(2)	1.3	0.39(23)	D	8	19 ⁻ → 18 ⁻	4598
400.0(2)	3.5			2	16 ⁺ → 15 ⁺	3017
403.8(2)	2.7	2.18(17) ^c	E2	11	9 ⁻ → 7 ⁻	1086
405.1(5)	0.1			5	15 ⁻ → 13 ⁻	2953
410.8(2)	2.7	0.79(22) ^c	M1	6	19 ⁻ → 18 ⁻	4507
412.9(3)	0.6			11	6 ⁻ → 7 ⁻	705
416.6(2)	25.8			1	13 ⁺ → 12 ⁺	1690
421.3(2)	0.8	1.65(67)	E2	4	11 ⁺ → 9 ⁺	1551
421.6(2)	1.9			6	20 ⁻ → 19 ⁻	4928
425.6(3)	0.8			7	20 ⁻ → 19 ⁻	5059
427.5(4)	0.1			6	15 ⁻ → 13 ⁻	3137
430.8(4)	0.5			5	14 ⁻ → 12 ⁻	2748
432.7(2)	1.1			7	19 ⁻ → 18 ⁻	4634
436.5(2)	3.1			2	16 ⁺ → 15 ⁺	3017
438.4(2)	6.5	0.50(22)	M1	5	20 ⁻ → 19 ⁻	4650
438.9(2)	1.4			3	15 ⁺ → 14 ⁺	2831
440.7(3)	1.3			1	21 ⁺ → 20 ⁺	5609
443.8(2)	1.1			1	16 ⁺ → 15 ⁺	3061
444.4(4)	0.7			5	16 ⁻ → 14 ⁻	3193
444.4(4)	0.2			13	13 ⁻ → 12 ⁻	2602
445.1(2)	1.3			3	16 ⁺ → 15 ⁺	3276
445.6(3)	0.5			3	17 ⁺ → 16 ⁺	3722
446.2(3)	0.9			5	13 ⁻ → 12 ⁻	2548
446.4(4)	0.2			5	13 ⁻ → 11 ⁻	2548
450.4(2)	0.8	0.59(28)	D	4	9 ⁺ → 10 ⁺	1130
451.1(2)	0.8	1.81(25) ^c	E2	13	9 ⁻ → 7 ⁻	1133
458.7(2)	3.8			1	11 ⁺ → 9 ⁺	967
459.5(3)	1.5			11	7 ⁻ → 7 ⁻	751
463.6(4)	0.1			11	14 ⁻ → 13 ⁻	2844
464.7(3)	0.7			9	10 ⁻ → 9 ⁻	1333
467.2(3)	2.1			2	18 ⁺ → 17 ⁺	3956
472.0(2)	3.6	0.68(19) ^c	M1	2	17 ⁺ → 16 ⁺	3489
473.4(3)	1.1			1	22 ⁺ → 21 ⁺	6082
473.5(4)	0.5			10	12 ⁻ → 11 ⁻	2046
474.4(3)	0.6			7	21 ⁻ → 20 ⁻	5533
475.9(3)	0.5			2	20 ⁺ → 19 ⁺	5022
476.2(4)	0.6			1	23 ⁺ → 22 ⁺	6558
476.4(2)	3.8			5	21 ⁻ → 20 ⁻	5126
477.3(4)	0.3			6	22 ⁻ → 21 ⁻	5912
479.5(4)	0.2			3	12 ⁺ → 11 ⁺	1784
479.9(5)	0.3			3	19 ⁺ → 18 ⁺	4713
480.3(2)	1.7			1	16 ⁺ → 15 ⁺	3061
482.1(2)	4.0			10	8 ⁻ → 6 ⁻	550
483.5(3)	0.2			<i>ls</i>	(9 ⁻) → (7 ⁻)	1281
492.8(2)	0.6			3	9 ⁺ → 10 ⁺	1172
495.7(2)	7.7	0.39(6)	M1	1	15 ⁺ → 14 ⁺	2581
499.5(3)	1.1			1	20 ⁺ → 19 ⁺	5168
500.6(4)	0.2			13	13 ⁻ → 12 ⁻	2602
504.7(2)	1.5	2.12(45) ^c	E2	11	10 ⁻ → 8 ⁻	1386
505.7(3)	1.2			6	21 ⁻ → 20 ⁻	5434
507.5(3)	0.3			6	16 ⁻ → 14 ⁻	3417
511.2(3)	0.7			3	18 ⁺ → 17 ⁺	4233
517.8(2)	2.4			5	22 ⁻ → 21 ⁻	5644
518.8(2)	0.8			2	9 ⁺ → 8 ⁺	933
521.8(2)	1.2			1	18 ⁺ → 17 ⁺	4129
523.9(4)	0.5			1	25 ⁺ → 24 ⁺	7610
528.0(4)	0.6			1	24 ⁺ → 23 ⁺	7086

TABLE I. (*Continued.*)

E_γ (keV)	I_γ	R_{DCO}	Mult.	Band _{<i>i</i>}	$I_i^\pi \rightarrow I_f^\pi$	E_i (keV)
529.8(3)	1.1			5	17 ⁻ → 15 ⁻	3483
532.1(2)	2.1			2	15 ⁺ → 14 ⁺	2617
539.1(3)	1.2			1	19 ⁺ → 18 ⁺	4669
540.7(2)	0.3			3	10 ⁺ → 8 ⁺	1306
546.5(2)	3.1	0.70(22)	M1	1	17 ⁺ → 16 ⁺	3608
549.9(3)	1.3			5	23 ⁻ → 22 ⁻	6194
558.5(2)	1.4			2	14 ⁺ → 13 ⁺	2248
560.4(5)	0.2			9	12 ⁻ → 11 ⁻	2133
561.4(3)	0.9			13	10 ⁻ → 8 ⁻	1468
562.5(4)	0.4			6	23 ⁻ → 22 ⁻	6474
572.6(3)	0.4			5	15 ⁻ → 13 ⁻	2953
574.1(3)	0.2			6	16 ⁻ → 14 ⁻	3417
575.3(4)	0.5			5	16 ⁻ → 15 ⁺	3193
576.6(2)	4.4	1.05(17)	E2	10	9 ⁻ → 7 ⁻	869
581.9(3)	0.2			10	14 ⁻ → 13 ⁻	2962
583.4(3)	0.6			3	11 ⁺ → 9 ⁺	1516
584.9(3)	1.2			9	8 ⁻ → 6 ⁻	653
590.3(3)	1.1			2	19 ⁺ → 18 ⁺	4547
592.2(3)	0.4			7	16 ⁻ → 15 ⁻	3545
592.6(3)	0.9			5	24 ⁻ → 23 ⁻	6787
594.1(2)	11.9			1	12 ⁺ → 10 ⁺	1273
599.0(3)	0.7			6	17 ⁻ → 15 ⁻	3736
607.1(3)	0.7			2	13 ⁺ → 11 ⁺	1911
608.9(4)	0.4			7	17 ⁻ → 15 ⁻	3861
610.6(2)	4.6	0.99(8)	E2	4	13 ⁺ → 11 ⁺	2161
612.1(4)	0.4			5	25 ⁻ → 24 ⁻	7399
613.5(3)	0.8			6	18 ⁻ → 17 ⁻	4096
614.1(4)	0.2	0.36(22)	D	12	7 ⁻ → 6 ⁻	682
617.6(3)	0.3			4	11 ⁺ → 9 ⁺	1551
620.4(2)	9.6	0.83(27) ^c	D	2	12 ⁺ → 11 ⁺	1587
624.8(2)	6.1			2	11 ⁺ → 10 ⁺	1304
626.6(3)	0.6			3	10 ⁺ → 10 ⁺	1306
629.6(2)	1.6			2	10 ⁺ → 9 ⁺	1138
633.0(3)	2.5			5	18 ⁻ → 16 ⁻	3826
633.3(2)	4.2	0.99(9)	E2	11	11 ⁻ → 9 ⁻	1719
633.7(3)	0.8			11	12 ⁻ → 10 ⁻	2101
637.9(2)	3.2	0.56(32)	D	2	13 ⁺ → 12 ⁺	1911
642.9(3)	0.8			9	9 ⁻ → 7 ⁻	1026
644.9(2)	3.5	0.93(8)	E2	4	13 ⁺ → 11 ⁺	2161
646.0(4)	0.1			3	12 ⁺ → 10 ⁺	1784
646.3(2)	3.5			13	11 ⁻ → 9 ⁻	1779
656.5(4)	0.2			7	18 ⁻ → 16 ⁻	4201
660.9(3)	0.2			2	14 ⁺ → 12 ⁺	2248
662.5(2)	0.9			5	14 ⁻ → 14 ⁺	2748
669.3(3)	0.4			6	16 ⁻ → 14 ⁻	3417
677.7(4)	0.6			11	13 ⁻ → 11 ⁻	2457
678.9(3)	0.5			6	18 ⁻ → 16 ⁻	4096
680.0(2)	0.7			6	15 ⁻ → 13 ⁻	3137
680.6(2)	1.9	2.17(38) ^c	E2	9	10 ⁻ → 8 ⁻	1333
680.8(4)	0.4			6	19 ⁻ → 18 ⁻	4507
682.9(3)	3.8			10	10 ⁻ → 8 ⁻	1233
683.6(4)	0.8			11	7 ⁻ → 6 ⁻	751
690.0(2)	0.7	1.27(49)	E2	13	12 ⁻ → 10 ⁻	2158
695.1(3)	0.7			2	21 ⁺ → 20 ⁺	5718
702.1(2)	0.5			5	14 ⁻ → 12 ⁻	2748
702.1(3)	2.4			3	14 ⁺ → 13 ⁺	2392
703.9(2)	6.1	1.08(16)	E2	10	11 ⁻ → 9 ⁻	1573
704.2(2)	2.1			5	15 ⁻ → 14 ⁺	2953

TABLE I. (Continued.)

E_γ (keV)	I_γ	R_{Dco}	Mult.	Band _{<i>i</i>}	$I_i^\pi \rightarrow I_f^\pi$	E_i (keV)
704.7(6)	0.8			3	$17^+ \rightarrow 16^+$	3722
706.3(4)	0.4			2	$15^+ \rightarrow 13^+$	2617
714.8(3)	2.3	2.31(40) ^c	<i>E2</i>	11	$12^- \rightarrow 10^-$	2101
716.2(5)	0.7			6	$20^- \rightarrow 19^-$	4928
718.5(3)	0.9			7	$18^- \rightarrow 17^-$	4201
723.1(2)	8.1			1	$13^+ \rightarrow 11^+$	1690
724.2(4)	0.5			2	$10^+ \rightarrow 8^+$	1138
729.1(3)	2.6	1.49(69)	<i>E2</i>	5	$19^- \rightarrow 17^-$	4212
729.5(3)	0.4			<i>1s</i>	$(7^-) \rightarrow 6^-$	797
730.2(3)	0.6			3	$13^+ \rightarrow 11^+$	2034
737.0(2)	0.8	0.93(28)	<i>E2</i>	8	$19^- \rightarrow 17^-$	4598
738.4(3)	3.6	0.95(11)	<i>E2</i>	11	$13^- \rightarrow 11^-$	2457
742.3(3)	1.9	1.02(35)	<i>E2</i>	11	$14^- \rightarrow 12^-$	2844
744.2(7)	0.3			3	$18^+ \rightarrow 17^+$	4233
745.7(5)	0.3			3	$15^+ \rightarrow 14^+$	2831
748.4(3)	0.4			6	$14^- \rightarrow 13^+$	2910
753.9(4)	0.4			13	$11^- \rightarrow 9^-$	1779
758.2(3)	0.3			3	$9^+ \rightarrow 8^+$	1172
760.5(3)	1.5			3	$13^+ \rightarrow 12^+$	2034
763.9(4)	0.2			5	$13^- \rightarrow 12^+$	2548
767.4(2)	8.1	1.06(13)	<i>E2</i>	4	$15^+ \rightarrow 13^+$	2929
768.2(2)	2.5			5	$13^- \rightarrow 11^-$	2548
769.3(3)	1.3			2	$16^+ \rightarrow 14^+$	3017
770.4(3)	0.6	2.66(52) ^c	<i>E2</i>	6	$19^- \rightarrow 17^-$	4507
771.4(3)	0.5			13	$12^- \rightarrow 10^-$	2158
783.6(5)	0.3			6	$17^- \rightarrow 15^-$	3736
783.7(3)	0.8			7	$18^- \rightarrow 16^-$	4201
783.7(5)	0.3			6	$21^- \rightarrow 20^-$	5434
785.3(4)	0.2			6	$22^- \rightarrow 21^-$	5912
795.8(2)	2.0			2	$11^+ \rightarrow 9^+$	1304
797.0(3)	0.5			3	$15^+ \rightarrow 13^+$	2831
797.6(4)	0.3			11	$14^- \rightarrow 12^-$	2844
797.9(3)	0.2			3	$9^+ \rightarrow 7^+$	1172
799.2(4)	1.2			9	$12^- \rightarrow 10^-$	2133
804.6(3)	0.8			3	$14^+ \rightarrow 12^+$	2392
807.0(2)	5.8			10	$13^- \rightarrow 11^-$	2380
808.5(4)	0.3			6	$14^- \rightarrow 12^-$	2910
812.2(2)	14.6			1	$14^+ \rightarrow 12^+$	2085
812.9(3)	3.3			10	$12^- \rightarrow 10^-$	2046
814.6(4)	0.4			11	$8^- \rightarrow 6^-$	882
816.8(2)	1.8			3	$12^+ \rightarrow 11^+$	1784
822.5(2)	4.6	1.00(13)	<i>E2</i>	4	$21^+ \rightarrow 19^+$	5444
822.6(2)	1.5	1.44(57)	<i>E2</i>	13	$13^- \rightarrow 11^-$	2602
824.3(3)	2.3			5	$20^- \rightarrow 18^-$	4650
824.5(3)	0.2			6	$14^- \rightarrow 14^+$	2910
825.3(4)	0.4			8	$21^- \rightarrow 19^-$	5459
829.6(6)	0.3			6	$23^- \rightarrow 22^-$	6474
832.2(4)	0.5			6	$20^- \rightarrow 18^-$	4928
836.8(2)	3.1			5	$14^- \rightarrow 13^+$	2748
837.0(3)	1.9	0.60(10)	<i>D</i>	3	$11^+ \rightarrow 10^+$	1516
844.6(4)	7.3	1.08(9)	<i>E2</i>	4	$19^+ \rightarrow 17^+$	4622
846.6(4)	0.4	1.93(87) ^c	<i>E2</i>	11	$15^- \rightarrow 13^-$	3304
848.3(4)	8.1	0.94(13)	<i>E2</i>	4	$17^+ \rightarrow 15^+$	3777
857.6(2)	4.6	1.40(52)	$\Delta I = 0$	5	$13^- \rightarrow 13^+$	2548
858.1(4)	0.4			7	$20^- \rightarrow 18^-$	5059
860.9(3)	1.7	1.68(37) ^c	<i>E2</i>	8	$21^- \rightarrow 19^-$	5459
861.5(5)	0.5	1.69(33) ^c	<i>E2</i>	8	$19^- \rightarrow 17^-$	4598
871.7(2)	1.5			4	$11^+ \rightarrow 10^+$	1551

TABLE I. (Continued.)

E_γ (keV)	I_γ	R_{Dco}	Mult.	Band _{<i>i</i>}	$I_i^\pi \rightarrow I_f^\pi$	E_i (keV)
872.1(3)	1.4			2	$17^+ \rightarrow 15^+$	3489
872.2(3)	1.3	0.93(15)	<i>E2</i>	7	$15^- \rightarrow 13^-$	3252
874.1(4)	0.5			9	$14^- \rightarrow 12^-$	3007
876.4(5)	0.2			6	$14^- \rightarrow 13^+$	2910
882.4(2)	3.5			4	$23^+ \rightarrow 21^+$	6327
883.1(2)	0.8			13	$13^- \rightarrow 11^-$	2602
884.3(3)	0.7			3	$16^+ \rightarrow 14^+$	3276
890.5(5)	0.2			3	$17^+ \rightarrow 15^+$	3722
891.3(2)	6.9	0.95(11)	<i>E2</i>	1	$15^+ \rightarrow 13^+$	2581
892.0(5)	0.2			3	$10^+ \rightarrow 8^+$	1306
899.3(6)	0.2			7	$21^- \rightarrow 19^-$	5533
906.5(3)	1.1	0.81(26)	<i>E2</i>	10	$15^- \rightarrow 13^-$	3286
907.9(2)	1.7			2	$12^+ \rightarrow 10^+$	1587
908.4(2)	1.0			2	$17^+ \rightarrow 15^+$	3489
914.1(3)	1.2			1	$22^+ \rightarrow 20^+$	6082
914.7(3)	2.3			5	$21^- \rightarrow 19^-$	5126
916.3(4)	0.8			10	$14^- \rightarrow 12^-$	2962
920.1(3)	0.8			3	$15^+ \rightarrow 13^+$	2831
923.7(5)	0.2			11	$15^- \rightarrow 13^-$	3304
927.4(4)	0.6			7	$16^- \rightarrow 15^+$	3545
927.6(2)	1.9			2	$15^+ \rightarrow 13^+$	2617
928.1(5)	0.4			6	$21^- \rightarrow 19^-$	5434
930.6(4)	0.2			5	$12^- \rightarrow 10^-$	2317
931.7(2)	2.4			2	$16^+ \rightarrow 14^+$	3017
939.0(3)	2.5			2	$18^+ \rightarrow 16^+$	3956
940.1(3)	1.5			1	$21^+ \rightarrow 19^+$	5609
945.1(4)	1.5			2	$13^+ \rightarrow 11^+$	1911
949.5(4)	0.8			1	$23^+ \rightarrow 21^+$	6558
956.8(4)	0.3			3	$18^+ \rightarrow 16^+$	4233
963.1(4)	0.3			7	$20^- \rightarrow 18^-$	5059
964.2(3)	1.7	1.07(31)	<i>E2</i>	8	$23^- \rightarrow 21^-$	6423
975.7(3)	8.1	0.94(17)	<i>E2</i>	1	$16^+ \rightarrow 14^+$	3061
977.3(2)	2.6			4	$25^+ \rightarrow 23^+$	7304
983.7(6)	0.6			6	$22^- \rightarrow 20^-$	5912
990.2(4)	0.6			1	$17^+ \rightarrow 15^+$	3608
990.8(5)	0.2			3	$19^+ \rightarrow 17^+$	4713
994.0(3)	1.8			5	$22^- \rightarrow 20^-$	5644
1004.3(4)	0.9			1	$24^+ \rightarrow 22^+$	7086
1015.2(5)	0.1			5	$11^- \rightarrow 9^-$	2101
1020.5(5)	0.2			6	$13^- \rightarrow 13^+$	2710
1026.5(4)	0.3			7	$21^- \rightarrow 19^-$	5533
1026.6(3)	4.0			1	$17^+ \rightarrow 15^+$	3608
1028.2(5)	0.9			3	$16^+ \rightarrow 14^+$	3276
1038.5(3)	2.7			1	$20^+ \rightarrow 18^+$	5168
1039.5(5)	0.2			6	$23^- \rightarrow 21^-$	6474
1043.9(3)	4.0			5	$12^- \rightarrow 12^+$	2317
1051.6(5)	0.7			1	$25^+ \rightarrow 23^+$	7610
1052.0(4)	0.3			6	$15^- \rightarrow 14^+$	3137
1057.2(4)	1.6			2	$19^+ \rightarrow 17^+$	4547
1060.9(3)	2.8			1	$19^+ \rightarrow 17^+$	4669
1062.7(4)	1.0			8	$25^- \rightarrow 23^-$	7486
1065.9(4)	2.1			2	$20^+ \rightarrow 18^+$	5022
1067.8(4)	1.5			5	$23^- \rightarrow 21^-$	6194
1068.0(3)	6.1			1	$18^+ \rightarrow 16^+$	4129
1074.7(3)	1.7			4	$27^+ \rightarrow 25^+$	8379
1075.1(5)	0.5			6	$24^- \rightarrow 22^-$	6987
1112.4(5)	0.7			1	$18^+ \rightarrow 16^+$	4129
1134.1(3)	1.1			5	$11^- \rightarrow 11^+$	2101

TABLE I. (*Continued.*)

E_γ (keV)	I_γ	R_{DCO}	Mult.	Band _{<i>i</i>}	$I_i^\pi \rightarrow I_f^\pi$	E_i (keV)
1142.7(5)	1.1			5	$24^- \rightarrow 22^-$	6787
1145.7(5)	0.4			1	$27^+ \rightarrow 25^+$	8756
1149.0(4)	0.7			8	$27^- \rightarrow 25^-$	8635
1154.0(5)	0.5			11	$14^- \rightarrow 13^+$	2844
1166.8(5)	1.2			4	$29^+ \rightarrow 27^+$	9545
1167.4(5)	0.8			7	$15^- \rightarrow 14^+$	3252
1170.6(5)	0.7			2	$21^+ \rightarrow 19^+$	5718
1191.0(5)	1.3			2	$22^+ \rightarrow 20^+$	6213
1191.2(6)	0.6			2	$23^+ \rightarrow 21^+$	6909
1204.8(5)	1.2			5	$25^- \rightarrow 23^-$	7399
1240.5(5)	0.4			8	$29^- \rightarrow 27^-$	9875
1251.2(5)	0.7			4	$31^+ \rightarrow 29^+$	10797
1260.8(7)	0.7			5	$26^- \rightarrow 24^-$	8048
1320.7(6)	0.4			5	$27^- \rightarrow 25^-$	8720
1328.7(5)	0.1			13	$13^- \rightarrow 12^+$	2602
1338.8(5)	0.2			8	$31^- \rightarrow 29^-$	11214
1349.3(7)	0.2			5	$28^- \rightarrow 26^-$	9397
1350.7(5)	0.2			4	$33^+ \rightarrow 31^+$	12147
1407.5(7)	0.2			5	$29^- \rightarrow 27^-$	10127
1436.6(5)	0.6			6	$13^- \rightarrow 12^+$	2710

^aMultipolarity was accepted from Ref. [43].

^bFor multipolarity assignment see the text.

^cDCO ratio was determined using a dipole gate.

The spin and parity assignments of the levels in band 12 are based on the known 2^- spin-parity of the ground state, the measured DCO ratios, and the internal conversion coefficients derived from the coincidence intensities. DCO ratios of all five low-energy transitions of band 12 indicate a stretched dipole character for these γ rays. In order to determine the $M1$ or $E1$ character of these transitions, their relative coincidence intensities seen in the double-gated coincidence spectra, obtained by setting gates on the 404-152 keV pair and the 404-131 keV pair, have been examined. In these spectra the relative total (γ -ray + conversion-electron) transition intensities for the 116-, 131-, 152-, 118-, and 164-keV transitions should be equal. By assuming an $M1$ character for the 164-keV γ ray, the relative total transition intensity in the cascade can be calculated, and the α_{tot} conversion coefficients of the other transitions can be derived by measuring their relative γ -ray intensities. This assumption can be justified: The 389- and the 451-keV transitions from the two lowest levels of band 13 have quadrupole character. As they have comparable intensities with the dipole transitions depopulating the same states, their multipolarity must be $E2$. Thus the initial and the final states of the 164-keV transition should have the same parity. The conversion coefficients are shown in Table II together with the theoretical conversion coefficients for $M1$ and $E1$ transitions.

It can be seen that the transitions have most likely $M1$ character, with some probable $E2$ admixture if the 164-keV transition is $M1$. In the last column of the table we show the conversion coefficients determined by assuming an $E1$ character for the 164-keV transition. In this case the experimental values lie halfway between the theoretical $E1$ and $M1$ values, which would imply an $E1$ transition with a

TABLE II. Conversion coefficients of dipole transitions in band 12. The theoretical α_{M1} and α_{E1} values are taken from Ref. [44]. The $\alpha_{\text{exp}}(1)$ values are derived with the assumption that the 164-keV transition is $M1$, while the $\alpha_{\text{exp}}(2)$ values are derived assuming an $E1$ character for it.

E_γ (keV)	α_{M1}	α_{E1}	$\alpha_{\text{exp}}(1)$	$\alpha_{\text{exp}}(2)$
115.7	0.86	0.17	0.97(29)	0.57(17)
117.9	0.81	0.16	0.86(26)	0.49(15)
131.3	0.60	0.12	0.81(24)	0.45(14)
152.5	0.39	0.08	0.65(19)	0.33(10)

strong $M2$ admixture. This scenario is not expected for these transitions because a strong $M2$ admixture would generate a significant lifetime, which was not observed. Thus the obtained conversion coefficients further confirm the assumption that the 164-keV transition has an $M1$ character. As all the dipole transitions in band 12 have stretched $M1$ character, all the levels in this band have negative parity and the spins of the consecutive levels must differ by $1\hbar$. We assign increasing spin values to the levels with increasing excitation energy for the following reasons.

- (i) The 11-min isomeric state is linked to the 5^- and 7^- levels of band 12 by stretched dipole transitions. If both of these spins were smaller, then the spin of the isomeric state would be smaller than or equal to $4\hbar$. In this case, however, there would be a possibility to decay to the ground state with a few orders of magnitude smaller lifetime than observed.
- (ii) If only the 7^- level had smaller spin value, and the spin of the 11-min isomeric state were $6\hbar$, then many inter-band decays would show an “unnatural” pattern, which is not expected between high-spin rotational bands. For example, if the spin of the highest-energy level of band 12 was $5\hbar$, then all the spins in band 11, and consequently in band 5, would be $2\hbar$ less than is plotted in the level scheme. In this case the lowest levels of band 5 would decay to band 1 by strong $M2$ transitions only, and not by $\Delta I = 0$ $E1$ transitions.

We note that the first excited low-spin state of ^{134}Pr reported in Ref. [45] has the same excitation energy within the experimental error as our 3^- level in band 12. Therefore, it is tempting to think that they are the same state. However, the spin assignment in Ref. [45] is 1^- . Thus either the two states are different or the spin assignment is not correct in one of the cases.

The spin of the 11-min isomeric state is fixed by the 332- and 614-keV stretched dipole transitions from band 12. It can only be $6\hbar$, which is in agreement with the value suggested tentatively in Ref. [43]. The parities of the bands in Fig. 2 are assigned by assuming that the quadrupole transitions which compete with dipole transitions from the same state are $E2$ transitions. Using this argument all the bands in Fig. 2 are proved to have negative parity. For the 11-min isomeric state it is in good agreement with the tentative parity assignment in Ref. [43]. The spins are assigned on the basis of the measured DCO ratios by assuming an increasing spin with increasing excitation energy within the bands.

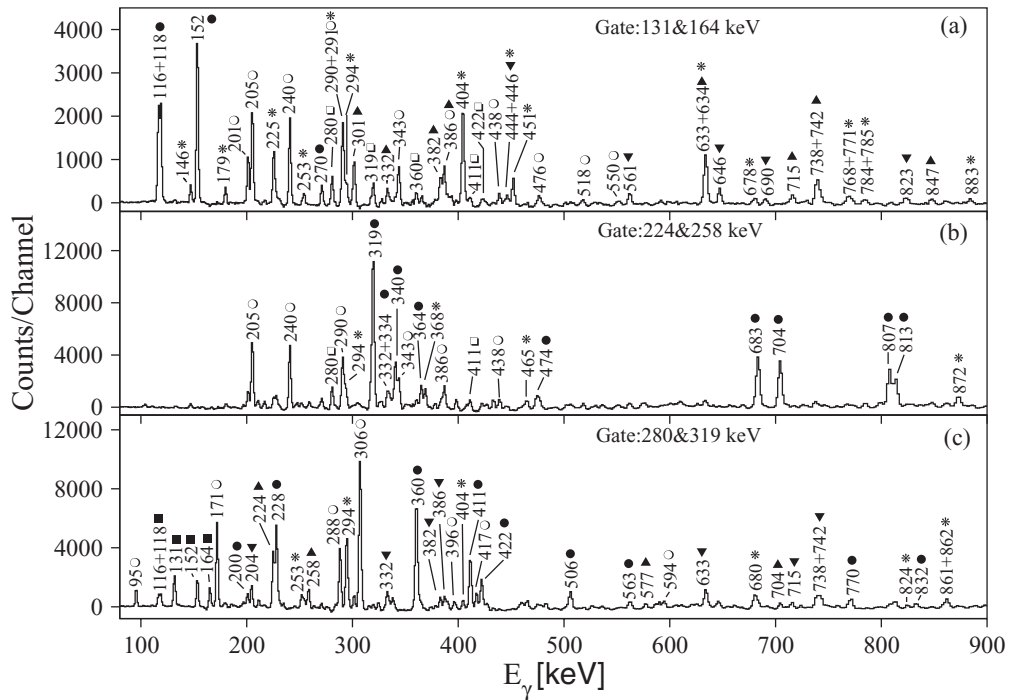


FIG. 1. Typical $\gamma\gamma$ -coincidence spectra obtained in the present work. In panel (a) the double gate was set on band 12 transitions. Peaks labeled with full circles, full upward triangles, and full downward triangles belong to bands 12, 11, and 13, respectively, while peaks labeled with open circles and open squares belong to bands 5 and 6, respectively. In panel (b) the double gate was set on band 10 transitions. Peaks labeled with full circles, open circles, and open squares belong to bands 10, 5, and 6, respectively. In panel (c) the double gate was set on band 6 transitions. Peaks labeled with full circles, full squares, full upward triangle, and full downward triangles belong to bands 6, 12, 10, and 11, respectively, while peaks labeled with open circles belong to band 1. Peaks labeled with stars in all the panels belong to transitions between bands.

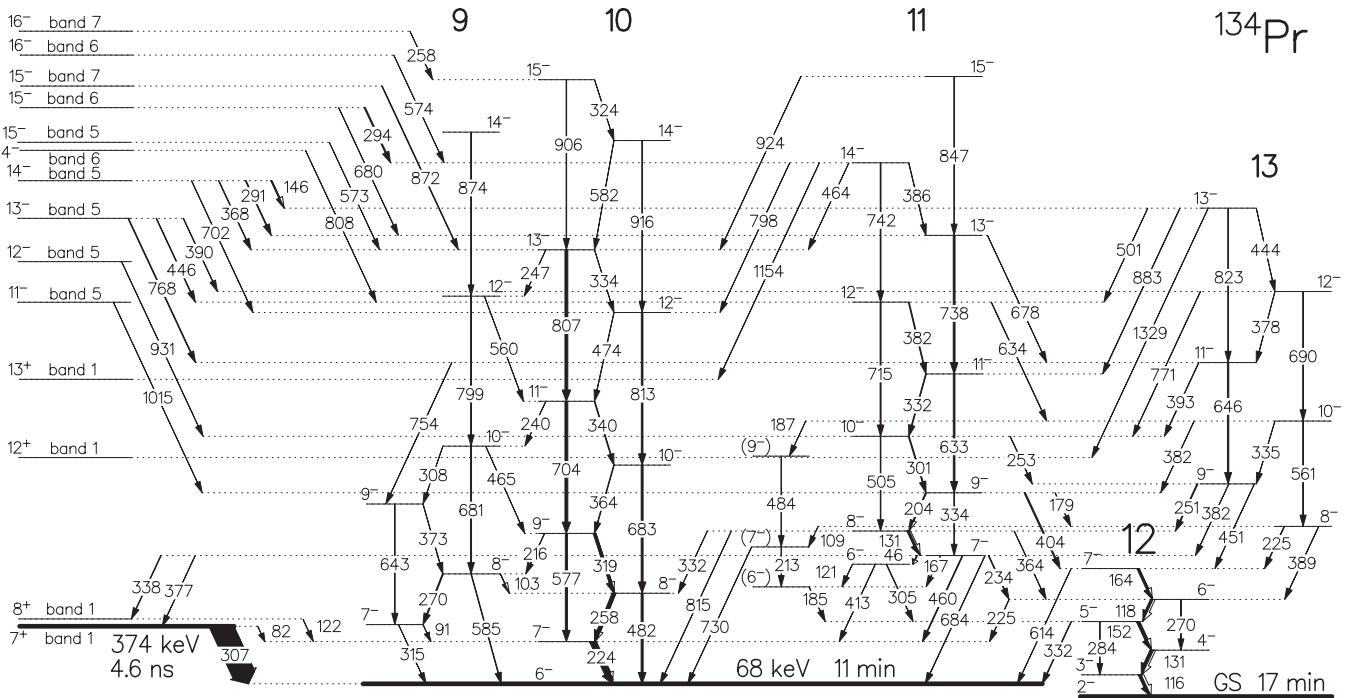


FIG. 2. Low- and medium-spin negative-parity bands of ^{134}Pr obtained in the present work. Linking transitions to the rest of the level scheme are plotted in the left side of the figure. The energies are given in keV, while the widths of the transitions are proportional to their relative intensities.

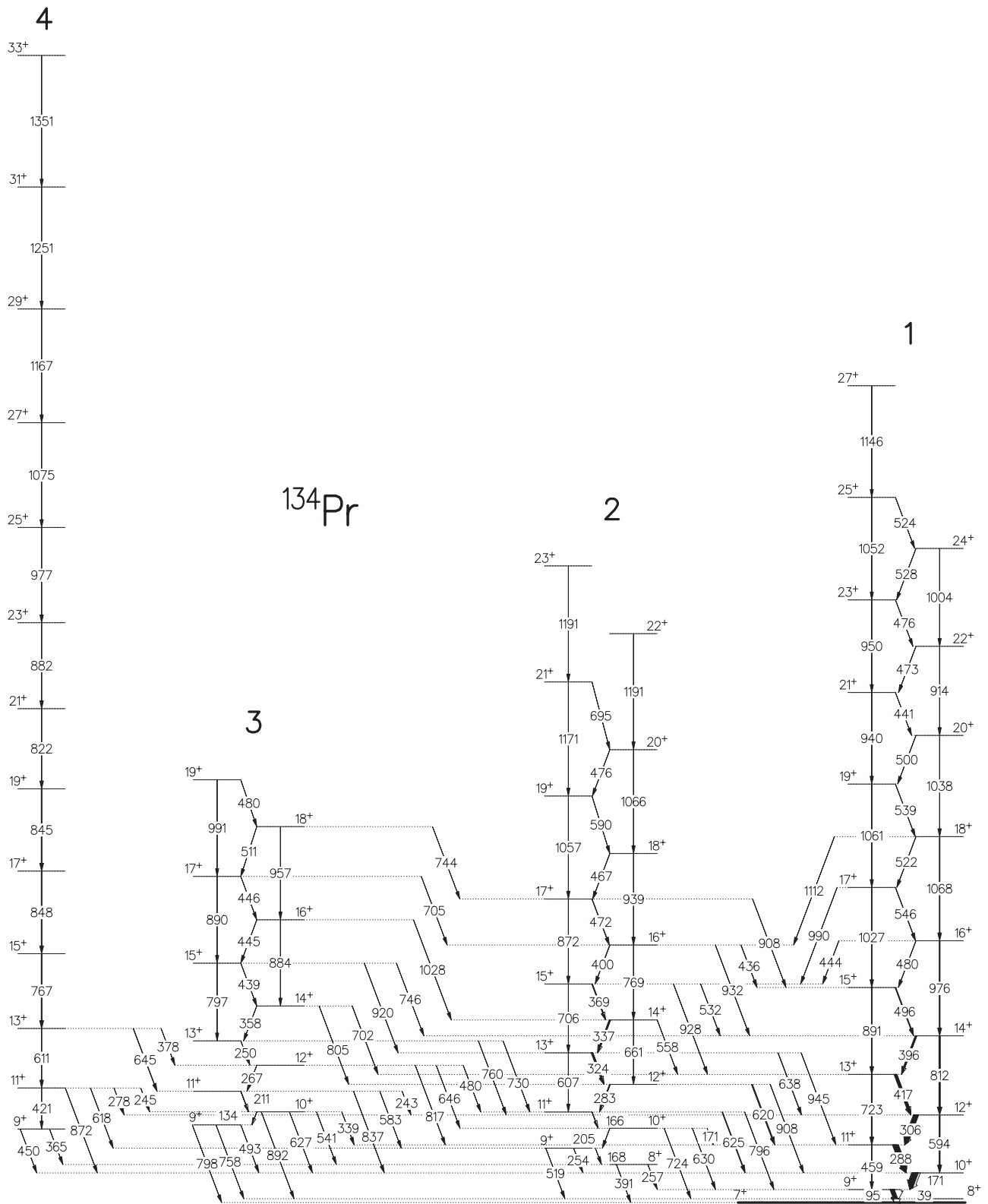


FIG. 3. Positive-parity bands of ^{134}Pr obtained in the present work. The energies are given in keV, while the widths of the transitions are proportional to their relative intensities.

Bands 11 and 13 have similar excitation energies and decay to each other through many dipole and quadrupole transitions, suggesting similar intrinsic structure. In addition,

the properties of bands 10 and 9 are similar to each other, although there are fewer linking transitions and only dipoles are seen. There is a small level structure containing three levels

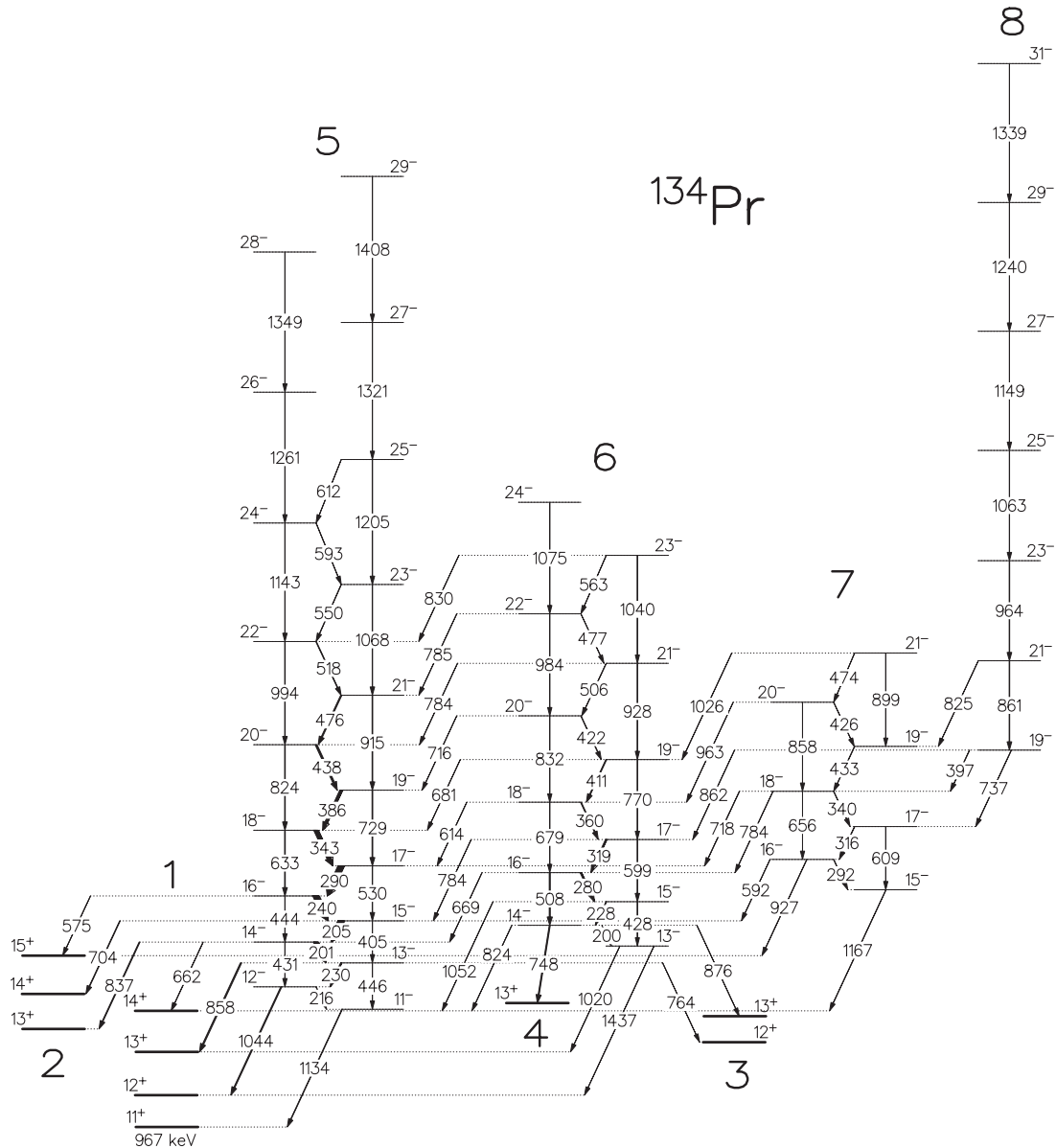


FIG. 4. High-spin negative-parity bands of ^{134}Pr obtained in the present work. In order to show the decays out to the positive-parity bands some levels of these bands are plotted by thick lines; however, the decays between these positive-parity levels are not plotted in this figure. The decays out to the negative-parity medium-spin bands are indicated in Fig. 2. The energies are given in keV, and the widths of the transitions are proportional to their relative intensities.

and linked mainly to bands 11, 12, and 13. It is placed in between bands 10 and 11 in Fig. 2.

B. Positive-parity bands

The positive-parity bands observed in the present experiment are plotted in Fig. 3. These bands decay to the short-lived 4.6-ns isomeric state, which was previously reported in Ref. [43]. Spin-parity 7^+ has been tentatively assigned to this level in Ref. [43]. It was possible to confirm this assignment from the present experimental data. The 307-keV transition from this level to the 6^- 11-min isomeric state has a stretched dipole character according to the measured DCO

ratio. Therefore the spin of the 4.6-ns level can be $7\hbar$ or $5\hbar$. In both cases its parity can be positive or negative. It is known from Ref. [43] that the 4.6-ns level is fed by a cascade of 39-, 95-, and 171-keV transitions, among which the first two have $M1$ character. In the present experiment we observed an 82-keV transition from the 4.6-ns level and a 122-keV transition from the level depopulating by the 39-keV transition. Both transitions go to the 7^- state of band 10, which decays to the 6^- state by a 224-keV transition (see Fig. 2). Examination of the relative coincidence intensities of the 95-, 82-, and 122-keV transitions in the coincidence spectrum double-gated on the 171- and 224-keV transitions can assist in deriving spin and parity values for the 4.6-ns state. The coincidence

TABLE III. Experimental coincidence γ -ray intensities derived from the spectrum double-gated by the 171- and 224-keV transitions, as well as calculated coincidence transition intensities assuming different spin-parity values for the 4.6-ns state. The theoretical conversion coefficient values are taken from Ref. [44].

E_γ (keV)	$I_{\gamma,\text{exp}}$	$I_{tr}(7^+)$	$I_{tr}(7^-)$	$I_{tr}(5^-)$	$I_{tr}(5^+)$
94.6	13(4)	33(10)	33(10)	33(10)	33(10)
82.4	19(6)	27(9)	62(20)	103(34)	550(180)
121.9	13(4)	15(5)	23(7)	23(7)	15(5)

γ -ray intensities can be obtained directly from the spectrum. The total transition intensities can be derived by taking into account the internal conversion coefficients, which depend on the multiplicities of the transitions and consequently on the spin and parity of the 4.6-ns state. In Table III we show the observed experimental γ -ray coincidence intensities for the 95-, 82-, and 122-keV transitions, as well as their calculated transition intensities for the four possible cases. In the case of the correct spin and parity the sum of transition intensities of the 82- and 122-keV transitions should be equal with the transition intensity of the 95-keV transition. As is seen in the table, only the 7^+ spin-parity complies with this condition. Thus, the spin-parity of the 4.6-ns state is 7^+ , which is in good agreement with the value tentatively suggested in Ref. [43].

The spin values of the higher-energy levels in Fig. 3 are derived using the multiplicities of the depopulating transitions obtained from the measured DCO ratios, by assuming that in the case of stretched transitions the spins increase with increasing excitation energy within a band. These spin assignments are confirmed also by the many linking transitions between the different bands, for all of which the experimental DCO ratios are consistent with the spin differences of the levels they connect. The parities of the bands are fixed by the quadrupole transitions that compete with dipole transitions from the same level. These transitions are considered to have $E2$ character. This argument provides positive parity for all four bands in Fig. 3. Bands 1, 2, and 4 have been reported previously, while band 3 was derived first from the data of the present experiment. This band is linked by many dipole and quadrupole transitions to bands 1 and 2.

C. High-spin negative-parity bands

The negative-parity high-spin bands observed for the present experiment are plotted in Fig. 4. Band 5 has been previously reported in Refs. [3,28]. The other bands in the figure are observed for the first time in our experiment. Bands 5, 6, and 7 decay both to the lower-energy parts of the positive-parity bands and to the medium-spin negative-parity bands. The experimental DCO ratios of these decay-out transitions, as well as those of the transitions within the bands and between the bands, unambiguously fix the spin and parity values of the levels. According to these assignments all the bands in Fig. 4 have negative parity. A unique feature of the decay out of band 5 is that it feeds band 1 only by $\Delta I = 0$ dipole transitions and band 2 only by stretched dipole transitions. Band 6 is linked

to band 5 by many stretched dipole transitions, while band 7 is linked to band 6 by many stretched quadrupole transitions.

IV. DISCUSSION

In this section we attempt to assign intrinsic single-particle configurations to the bands in ^{134}Pr . Measured $B(M1)/B(E2)$ ratios, alignments, band-crossing frequencies, bandhead spins, and the single-particle configurations in the neighboring nuclei, as well as the predictions of total Routhian surface (TRS) and tilted-axis cranking (TAC) calculations are used to determine the configurations.

According to the observed intrinsic configurations in ^{132}Ce and neighboring odd- A nuclei, the active single-particle states in ^{134}Pr are the $[541]3/2^-$, $[411]3/2^+$, and $[413]5/2^+$ proton states, as well as the $[514]9/2^-$, $[400]1/2^+$, $[660]1/2^+$ and $[404]7/2^+$ neutron states. Indeed, Ref. [46] reports on bands based on the rotation-aligned $[541]3/2^-$ Nilsson state of $h_{11/2}$ parentage, as well as bands based on the deformation-aligned $[411]3/2^+$, and $[413]5/2^+$ states of $d_{5/2}$ and $g_{7/2}$ parentage, respectively, in ^{133}Pr . Similarly, Ref. [47] reports on a band based on the $[400]1/2^+$ state derived from the $s_{1/2}$ subshell, bands based on the deformation-aligned $[514]9/2^-$ state derived from the $h_{11/2}$ subshell, and a band based on the rotation-aligned $[660]1/2^+$ state of $i_{13/2}$ parentage in ^{133}Ce . Furthermore, previous experimental results on ^{134}Pr suggest the possible presence of the $[541]1/2^-$ or $[530]1/2^-$ intruder neutron orbitals [3], while the presence of the $[404]7/2^+$ neutron orbital was reported in Ref. [48]. In the case of the odd-odd ^{134}Pr we expect bands that are based on the combinations of the above single-proton and single-neutron states.

A. Analysis of the $B(M1)/B(E2)$ ratios

In order to assist in the configuration assignments we have derived the experimental in-band $B[M1; I \rightarrow (I-1)]/B[E2; I \rightarrow (I-2)]$ ratios for the $\Delta I = 1$ bands using the expression

$$\frac{B(M1; I \rightarrow I-1)}{B(E2; I \rightarrow I-2)} = 0.697 \frac{E_\gamma^5(E2)}{E_\gamma^3(M1)} \frac{I_\gamma(M1)}{I_\gamma(E2)} \frac{1}{1+\delta^2} \left(\frac{\mu_N}{eb}\right)^2, \quad (1)$$

where the energies of the γ rays are given in MeV. The δ -multipole mixing ratios of the $\Delta I = 1$ transitions were assumed to be small, and thus δ^2 can be neglected. The experimental $B(M1)/B(E2)$ ratios were compared to calculated values obtained using a generalized expression of the geometrical model of Dönau and Frauendorf [49], formulated in Refs. [50,51]. In the calculation, the K and i_x values were approximated with constant values, and these are listed in Table IV together with the appropriate g values taken from [52]. The rotational gyromagnetic factor was taken as $g_R = Z/A$, while the Q_0 electric quadrupole moments and the γ shape parameters were derived from the nuclear shape predicted by the TRS calculations. As the results of the TRS calculations failed to reproduce satisfactorily

TABLE IV. Parameters used for the calculation of $B(M1)/B(E2)$ ratios.

Configuration	g factor	K value	i_x
$\pi h_{11/2}$	1.33	1.5	4.5
$\pi g_{7/2}$	0.75	2.5	1.5
$\pi d_{5/2}$	1.40	1.5	1.5
$\nu h_{11/2}$	-0.18	4.5	2
$\nu s_{1/2}$	-1.27	0.5	0
$\nu g_{7/2}$	0.3	3.5	1

the experimental results, the obtained shape parameters are ambiguous. Moreover, within the TRS there is no tilted axis cranking possible, which is expected in this nucleus. Nevertheless, it is expected that the calculated $B(M1)/B(E2)$ ratios still can serve as a guide in the configuration assignment, as there can be large differences (an order of magnitude or more) between the $B(M1)/B(E2)$ ratios of the different configurations. Because of this approximate treatment of the calculated values, the signature splitting was not taken into account in the calculations.

The experimental and calculated $B(M1)/B(E2)$ ratios are compared in Fig. 5. Although all the possible configurations were taken into account in the calculations, only the configurations with calculated $B(M1)/B(E2)$ ratios reasonably close to the experimental values are plotted. For the possible configurations not shown, the calculated values differ from the experimental ones by about an order of magnitude or more.

B. Analysis of the alignments and Routhians

In order to confirm and further specify the assigned configurations, we have also derived the experimental alignments (i_x) and Routhians (e') of the bands as they are defined in [53] and plotted them in Fig. 6. A rotational reference, with a variable moment of inertia $J_{\text{ref}} = J_0 + \omega^2 J_1$, has been subtracted with Harris parameters $J_0 = 12\hbar^2 \text{ MeV}^{-1}$ and $J_1 = 29\hbar^4 \text{ MeV}^{-3}$ (as in Ref. [3]). In the derivation we assumed a $K = 6$ value for the bands 1, 2, 3, 5, 6, 7, 9, 10, 11, and 13. $K = 1$ was assumed for the doubly decoupled bands 4 and 8, and $K = 2$ for band 12.

The experimental total Routhians (E') and aligned total angular momenta (I_x) are also compared to the TRS calculations based on the Woods-Saxon cranking formalism [54–56]. The labeling of the TRS orbitals is given in Table V. The compared values are plotted in Fig. 8 for the negative-parity two-quasiparticle bands. The Routhians are normalized by adding the same constant value to all the experimental configurations in a way that the predicted and experimental values for band 10 are consistent at $\hbar\omega \approx 0.25 \text{ MeV}$.

C. Band configurations

1. The positive-parity bands

The configuration and the possible chiral nature of bands 1 and 2 have been thoroughly discussed in several previous papers [1,4,9,23–27]. According to these results bands 1 and

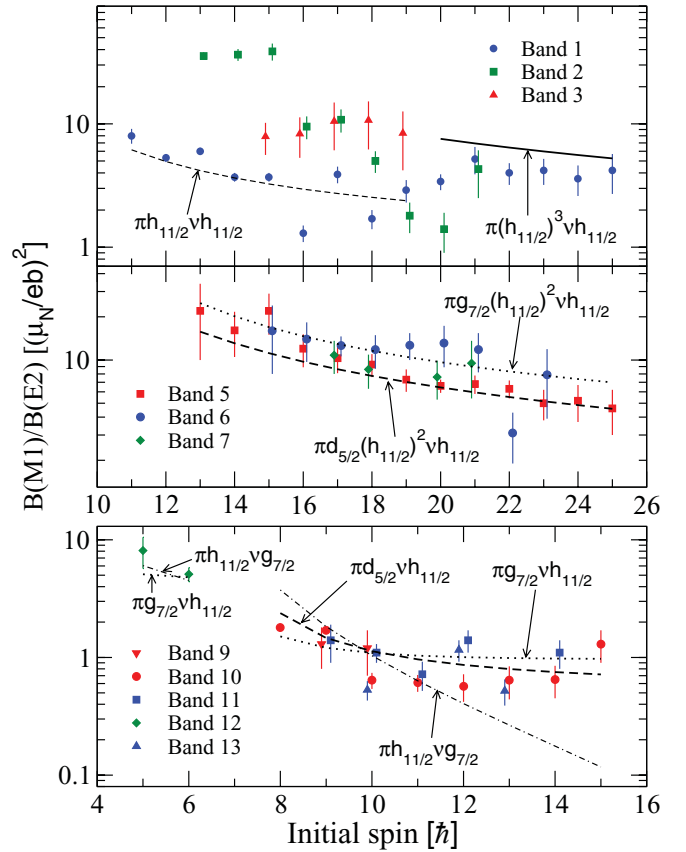


FIG. 5. (Color online) Experimental $B(M1)/B(E2)$ ratios of the ^{134}Pr bands obtained in the present work compared with calculated values assuming different configurations.

2 both have $\pi h_{11/2}\nu h_{11/2}$ configurations. In the present work, we confirm the previous tentative spin assignments; however, no new significant experimental data could be derived for these bands, which would affect the previous assignments and theoretical considerations. Thus we accept the previous interpretations.

Band 4 was discussed in Refs. [27,29,30] and has been suggested to correspond to the $\pi h_{11/2}\nu(f_{7/2}, h_{9/2})$ configuration below the first alignment frequency. The $f_{7/2}$ and $h_{9/2}$ neutron orbitals, corresponding to the [530]1/2 and [541]1/2 Nilsson states, are strongly mixed in this region. Without

TABLE V. Labels used for the quasiproton (p) and quasineutron (n) states of parity π and signature α ; n denotes the n th state for a given set of (π, α) quantum numbers.

p			n		
$(\pi, \alpha)_n$	Label	Shell model	$(\pi, \alpha)_n$	Label	Shell model
$(+, +1/2)_1$	A	$d_{5/2}, g_{7/2}$	$(+, +1/2)_1$	a	$g_{7/2}$
$(+, -1/2)_1$	B	$d_{5/2}, g_{7/2}$	$(+, -1/2)_1$	b	$g_{7/2}$
$(+, +1/2)_2$	C	$d_{5/2}, g_{7/2}$	$(-, -1/2)_1$	e	$h_{11/2}$
$(+, -1/2)_2$	D	$d_{5/2}, g_{7/2}$	$(-, +1/2)_1$	f	$h_{11/2}$
$(-, -1/2)_1$	E	$h_{11/2}$			
$(-, +1/2)_1$	F	$h_{11/2}$			
$(-, -1/2)_2$	G	$h_{11/2}$			

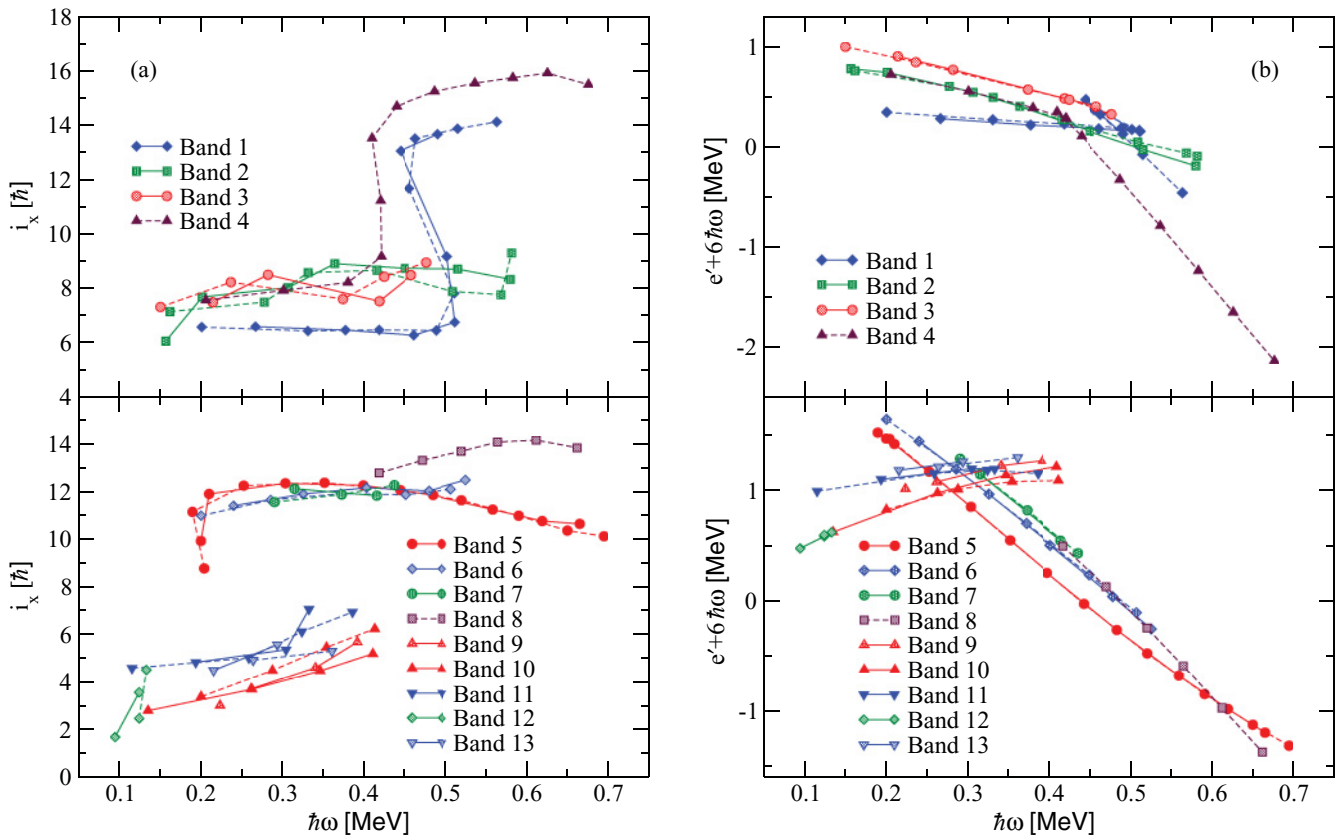


FIG. 6. (Color online) Alignments (a) and Routhians (b) of the bands observed in the present experiment as a function of the rotational frequency. Experimental points connected by solid (dashed) lines correspond to the even-spin (odd-spin) branch of the band.

mixing, the coupling of the $[530]1/2$ neutron Nilsson orbital with the $[541]3/2$ proton Nilsson orbital would lead to a doubly decoupled band having odd-spin states, while the $[541]1/2$ neutron Nilsson state would generate an even-spin band. Petrache *et al.* [27] assigned odd spins to this band, and therefore a $\pi h_{11/2} \nu [530]1/2$ configuration was suggested. On the other hand, Hauschild *et al.* [29] assigned even spins to the states in band 4 on the basis of the measured DCO ratios for the linking transitions between bands 4 and 1. Later Roberts *et al.* [43] increased the spin values of the band 1 states by 1 unit, which led again to odd-spin states in band 4. According to the present results, the states have odd spins. Therefore, most probably the main component of the configuration of band 4 is $\pi h_{11/2} \nu [530]1/2$. This assignment is also in good agreement with the measured bandhead spin of $9\hbar$, which is the sum of the single-particle spins expected for the rotation-aligned $f_{7/2}$ neutron and $h_{11/2}$ proton.

The alignment around $\hbar\omega = 0.45$ MeV in bands 1 and 4 has been thought to correspond to the proton FG crossing in the previous assignments [27,29] on the basis of TRS calculations and the observed alignment gain. The predicted FG crossing frequency is about $\hbar\omega = 0.5$ MeV. The lower observed crossing frequency ($\hbar\omega = 0.41$ MeV) for band 4 was attributed to a reduced pairing strength due to blocking of the first $\pi h_{11/2}$ proton crossing [29]. However, in this case the crossing frequency for band 1 would also be reduced. In the case of band 4 the neutron ef crossing is also possible,

and it is expected to be characterized by a similar alignment gain to that of the proton FG crossing, however at a lower rotational frequency. The $B(M1)/B(E2)$ ratios observed in the present experiment for the upper part of band 1 confirm the FG crossing scenario for band 1, while the lower crossing frequency favors the neutron ef crossing scenario in the case of band 4. We need to mention, however, that although both the ef and FG crossings are expected to occur in band 4, only one crossing is observed up to $\hbar\omega = 0.65$ MeV. The reason for this inconsistency is not clear. A possible explanation might be that due to the gamma softness of ^{134}Pr the ef crossing drives the nuclear shape to triaxial characterized by a negative gamma value, which pushes the FG crossing to higher rotational frequency.

Band 3 is newly identified in the present work. This $\Delta I = 1$ band has positive parity, and it decays through several $M1$ and $E2$ transitions to bands 1 and 2. It has an alignment value of around $8\hbar$, which corresponds to a two-quasiparticle configuration. These facts indicate that its configuration is $\pi h_{11/2} \nu h_{11/2}$, similar to the configuration of bands 1 and 2. The observed $B(M1)/B(E2)$ ratios of band 3 are two to three times larger than the corresponding ratios of band 1 and are close to the $B(M1)/B(E2)$ ratios of band 2 near the $17\hbar$ spin region. This suggests a similarity between bands 2 and 3, which might indicate that the two bands are chiral partners. In this context, it may be informative to inspect also the signature splittings of the three $\pi h_{11/2} \nu h_{11/2}$ bands. In the

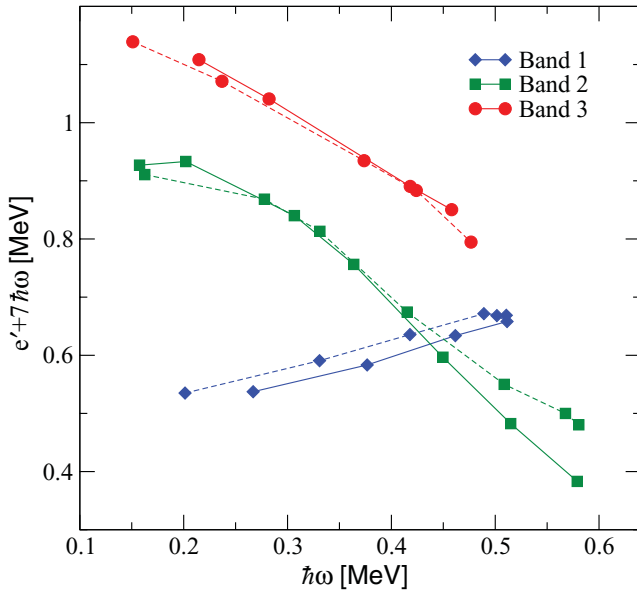


FIG. 7. (Color online) Observed signature splittings for the three positive-parity $\Delta I = 1$ bands.

case of chiral geometry a small signature splitting is expected for the bands in the region of stable chirality. (Although the signature is not a good quantum number in the chiral case, we still use here the expression “signature splitting” for the observed odd-even staggering.) Thus, it is also a test for the chiral scenario. In Fig. 7, the Routhians for bands 1, 2, and 3 are plotted below the first alignment in band 1. Band 1 shows a constant ~ 30 -keV signature splitting through the whole plotted frequency region, while the signature splittings of the two other bands are very small, being less than 10 keV in the $\hbar\omega = 0.3$ – 0.4 MeV frequency region. This fact might show that if there are chiral doublet bands among these three bands, the doublet is not bands 1 and 3, but rather bands 2 and 3. This scenario seems to be also confirmed by the very similar alignment values for bands 2 and 3, while band 1 has a considerably smaller alignment value. Moreover, the signature splitting for band 1 is inverted. Low-spin signature inversion occurs systematically in this mass region for the $\pi h_{11/2} \nu h_{11/2}$ bands [57]. The exact cause is still not understood completely; however, it has been suggested that both the triaxial shape of the nucleus and the proton-neutron residual interaction play a significant role. It is expected when the nuclear shape is triaxial with a positive γ value corresponding to the Lund convention [58]. This corresponds to the rotation around the small deformation axis instead of the medium axis, which would correspond to the chiral scenario. However, we stress again that the cause of the signature inversion is not well known yet, and thus we cannot draw strong conclusions on the shape of the nucleus only on the basis of the signature inversion.

2. The negative-parity two-quasiparticle bands

Bands 9–13 were not known before the present work. Their small alignment values in Fig. 6 indicate that they correspond to two-quasiparticle states. They are all $\Delta I = 1$ bands with

negative parity. Thus, they should correspond to either the $\pi[541]3/2\nu[400]1/2$ or $[404]7/2$ or the $\pi([413]5/2$ or $[411]3/2)\nu[514]9/2$ configurations.

It would be straightforward to think that these bands correspond to the lowest-energy first few negative-parity configurations predicted by the TRS calculations. In Fig. 8 we compared the experimental Routhians and aligned angular momenta of bands 9–13 with that of the low-energy negative-parity TRS configurations. The lowest experimental Routhians belong to band 12 at the lowest frequencies, and they belong to bands 9 and 10 at higher frequencies. It is the (Ea,Eb) TRS configuration pair that is predicted to have the lowest Routhians up to about $\hbar\omega = 0.25$ MeV. By taking into account that this configuration corresponds to a semidecoupled band, and given that no band similar to band 12 has been observed, band 12 could correspond to this configuration. The observed and calculated $B(M1)/B(E2)$ ratios are also in good agreement with this assignment. However, there are features which contradict this assumption. One is the signature splitting. Very small signature splitting is observed in band 12, while quite large signature splitting (around 100 keV) is expected for the (Ea,Eb) TRS configurations, although the predicted signature splitting depends strongly on the γ deformation parameter and the nucleus is very γ soft. A more serious discrepancy is related to the observed and predicted alignment values. At a rotational frequency of $\hbar\omega \approx 0.1$ MeV the predicted alignment value is around $6\hbar$, reflecting the rotation-aligned nature of the $h_{11/2}$ proton, while the observed alignment is only around $3\hbar$, suggesting a configuration without the rotation-aligned $h_{11/2}$ proton orbital.

Indeed, the bandhead of band 12 has a spin value of $2\hbar$. Such a small bandhead spin cannot be built from a configuration that contains the rotation-aligned $[541]3/2^-$ proton state. Thus, the possible configuration of this band is either $\pi[413]5/2\nu[514]9/2$ or $\pi[411]3/2\nu[514]9/2$, both of which contain deformation-aligned orbitals. According to the Gallagher-Moskowsky rule [59], the bandhead spin of the first configuration would be $2\hbar$, while the bandhead of the second configuration is expected to have $6\hbar$ spin. Thus, it is a sensible assumption that band 12 corresponds to the $\pi[413]5/2\nu[514]9/2$ configuration. The calculated $B(M1)/B(E2)$ ratios for the $\pi g_{7/2} \nu h_{11/2}$ configuration also reproduce the experimental values quite well.

Bands 9 and 10 are $\Delta I = 1$ bands linked to each other by several γ transitions, which indicates that they may correspond to two-quasiparticle configurations built up from deformation-aligned proton and neutron orbitals. The situation is the same for bands 11 and 13. Thus, the probable configurations of these bands are $\pi[413]5/2\nu[514]9/2$ or $\pi[411]3/2\nu[514]9/2$. The calculated $B(M1)/B(E2)$ ratios for both the $\pi g_{7/2} \nu h_{11/2}$ and $\pi d_{5/2} \nu h_{11/2}$ configurations reproduce reasonably well the observed ratios of all four bands, as the experimental values of the different bands are very similar. Although the calculated $B(M1)/B(E2)$ ratio values for the $\pi h_{11/2} \nu g_{7/2}$ configuration are also relatively close to the experimental values, this configuration assignment is not that probable because the slope of the calculated curve is quite different from that of the experimental values as a function of spin. Moreover, this configuration contains the rotation-aligned (decoupled)

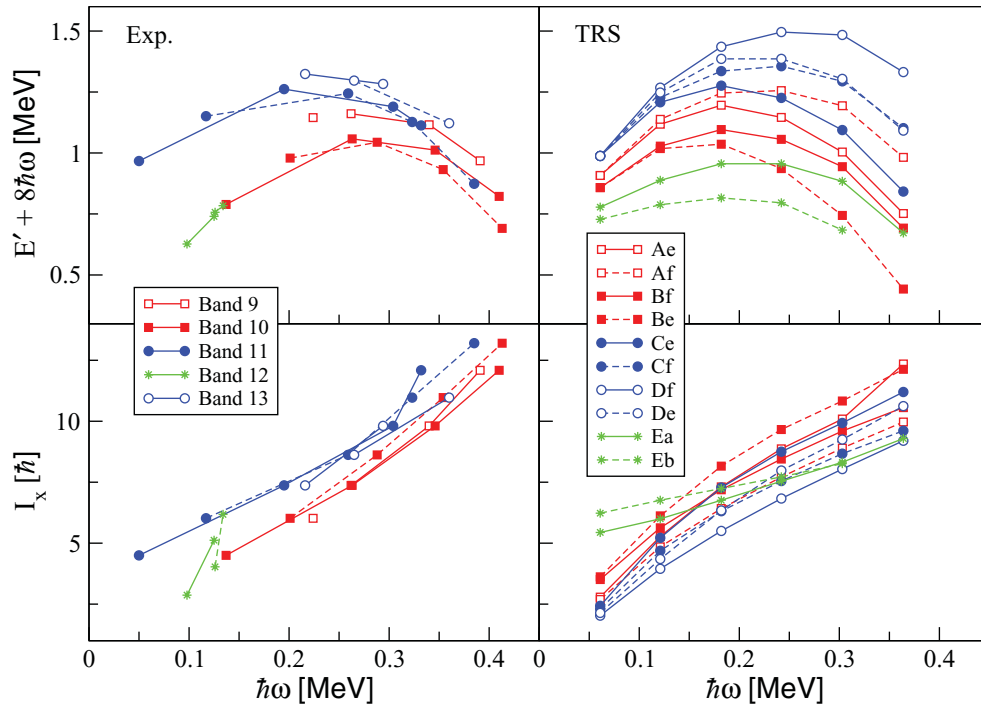


FIG. 8. (Color online) Comparison of the experimental Routhians (E') and aligned angular momenta (I_x) of the two-quasiparticle negative-parity bands with that predicted by the TRS calculations for the lowest-lying negative-parity configurations.

$\pi[541]3/2^-$ proton orbital, for which only one $\Delta I = 1$ band would be expected.

The four lowest-energy negative-parity TRS configurations without the $h_{11/2}$ proton orbital are the Be, Bf, Ae, and Af configurations. The relative positions of the predicted Routhians of these configurations are in reasonable agreement with the observed Routhians for bands 9 and 10. The predicted alignments are also reasonably close to the observed ones. Hence, (Be,Bf) and (Ae,Af) are good candidates for the configurations of bands 10 and 9, respectively. These configurations are predicted to have shape parameters around ($\beta_2 = 0.2, \gamma = -30^\circ$), although with a very shallow minimum as a function of the γ parameter, and other local minima ($\beta_2 \approx 0.2, \gamma \approx +20^\circ$) and ($\beta_2 \approx 0.2, \gamma \approx -90^\circ$) are predicted within a few hundred keV. The A and B TRS states can correspond to either the $\pi[413]5/2$ or the $\pi[411]3/2$ Nilsson orbitals. Because of the several possible shapes, it is difficult to unambiguously identify the corresponding Nilsson orbital; however, the spin value of the bandhead state of band 10 might provide a clue. The K value for the $\pi[411]3/2\nu[514]9/2$ configuration is expected to be 6 or 3, with 6 being the favored one, while in the case of the $\pi[413]5/2\nu[514]9/2$ configuration the expected K values are 7 and 2, with 2 being favored. Thus, bands 9 and 10 probably correspond to the $\pi[411]3/2\nu[514]9/2$ Nilsson configuration.

One could expect that the bands 11 and 13 doublet corresponds to the Ce, Cf, Df, and De TRS configurations, which are the next negative-parity configurations not involving the proton $h_{11/2}$ orbital. However, the predicted features of these configurations do not agree with the observed features of the bands 11 and 13 doublet. In contrast with the predictions, the observed aligned angular momenta of these bands are not

smaller than that observed for bands 9 and 10, but rather larger by $2\hbar$. Thus, also in contrast with the predictions, the Routhians of the two doublets converge with increasing rotational frequency instead of diverging. These features are expected for the case of bands in which the γ phonon is coupled to the configurations of bands 9 and 10, rather than in the case of the Ce, Cf, Df, and De TRS configurations. This assumption is in line with the fact that the nucleus in the Ae, Af, Bf, and Be TRS configurations is predicted to be rather γ soft. Bands in which the γ phonon is coupled to the yrast band are observed also in ^{132}Ce [48] and ^{133}Pr [60] with a γ -phonon energy of around 0.5 MeV. In the present case the bandhead energy difference between band 11 and band 10 is close to this value. Therefore, bands 11 and 13 might correspond to the configurations in which a γ phonon is coupled to the configurations of bands 9 and 10, or in which these configurations are mixed with the Ce, Cf, Df, and De TRS configurations.

3. The negative-parity four-quasiparticle bands

Bands 5, 6 and 7 are $\Delta I = 1$ bands linked to each other by several γ transitions, suggesting similar configurations. These bands cross bands 9, 10, 11, and 13 at a frequency of around $\hbar\omega = 0.3$ MeV, with an alignment gain of about $8\hbar$. These crossing frequency and alignment values are close to those predicted by cranked shell-model calculations for the alignment of the first proton pair. On the other hand, the observed $B(M1)/B(E2)$ ratios can only be reproduced by the present geometrical model calculations, if the configuration is either $\pi d_{5/2}(h_{11/2})^2\nu h_{11/2}$ or $\pi g_{7/2}(h_{11/2})^2\nu h_{11/2}$. On the basis of these facts, we can assume that the configurations of bands

5, 6, and 7 correspond to the above configurations. However, on the basis of the available data we cannot decide which of the above two configurations belong to which band. In the case of band 5, this configuration assignment is in good agreement with that proposed in Ref. [3].

Band 8 is a doubly decoupled negative-parity band. Another doubly decoupled, tentative negative-parity band has already been observed in this nucleus [29,30] and assigned as having $\pi h_{11/2} \nu i_{13/2}$ configuration. We also see another band with an intensity of about 1.5 times that of the band 8 intensity; however, we could not link it to the level scheme. The levels belonging to this unlinked band have tentative even spin values in good agreement with the fact that the expected favored signature branch of the [660]1/2 ($i_{13/2}$) neutron orbital is the $\alpha = +1/2$ branch, while for the [541]3/2 ($h_{11/2}$) proton orbital it is the $\alpha = -1/2$ branch. The levels of band 8 have odd spin values. Thus this band may correspond to the $\pi h_{11/2} \nu i_{13/2}$ configuration either with the $\alpha = +1/2$ branch or with the $\alpha = -1/2$ branch in both orbitals. The signature splitting is predicted to be smaller for the proton orbital, and thus band 8 probably corresponds to the above configuration with $\alpha = +1/2$ signature in both orbitals.

V. SUMMARY

The high-spin structure of the ^{134}Pr nucleus has been studied using the $^{116}\text{Cd}(^{23}\text{Na}, 5n)$ reaction in order to search for new rotational bands and obtain a more complete picture of the structure and special features of this nucleus. The level scheme of ^{134}Pr has been extended from this work. Nine new rotational bands have been found, among which one positive-parity band might be the chiral-partner candidate of the yrare $\pi h_{11/2} \nu h_{11/2}$

band, while five of them are the expected two-quasiparticle negative-parity bands. The relative placement of the two previously known isomeric states has been established, and thus the ground state of the nucleus has been unambiguously determined. According to the present results, the 2^- (17-min) state is the ground state and the 6^- (11-min) state is the excited state at 68 keV above the ground state. The tentatively assigned spin and parity values of the previously known states have been unambiguously determined.

Experimental Routhians and aligned angular momenta, as well as $B(M1)/B(E2)$ ratios, have been derived from the data and compared with predictions of total Routhian surface calculations, and results of the geometrical model of Dönau and Frauendorf, respectively. On the basis of these comparisons, and on the basis of comparison with neighboring nuclei, tentative configurations have been assigned to the new bands. According to this assignment, the observed negative-parity two-quasiparticle bands have a $\pi(g_{7/2}/d_{5/2})\nu h_{11/2}$ configuration, and a configuration in which $\pi(g_{7/2}/d_{5/2})\nu h_{11/2}$ is coupled to a γ phonon. This observation confirms the γ -soft behavior of ^{134}Pr , which is in line with the possible role of shape fluctuations proposed in Ref. [23].

ACKNOWLEDGMENTS

This work was supported in part by the Hungarian Scientific Research Fund, OTKA (Contract No. K72566), the Natural Sciences and Engineering Research Council of Canada under Contract No. SAPIN/371656-2010, the Bolyai János Foundation, the US National Science Foundation, the US Department of Energy, and the UK Engineering and Physical Sciences Research Council.

-
- [1] S. Frauendorf and J. Meng, *Nucl. Phys. A* **617**, 131 (1997).
 [2] V. I. Dimitrov, S. Frauendorf, and F. Dönau, *Phys. Rev. Lett.* **84**, 5732 (2000).
 [3] C. M. Petrache, D. Bazzacco, S. Lunardi, C. Rossi Alvarez, G. de Angelis, M. De Poli, D. Bucurescu, C. A. Ur, P. B. Semmes, and R. Wyss, *Nucl. Phys. A* **597**, 106 (1996).
 [4] K. Starosta *et al.*, *Phys. Rev. Lett.* **86**, 971 (2001).
 [5] A. A. Hecht *et al.* *Phys. Rev. C* **63**, 051302(R) (2001).
 [6] D. J. Hartley *et al.*, *Phys. Rev. C* **64**, 031304(R) (2001).
 [7] T. Koike, K. Starosta, C. J. Chiara, D. B. Fossan, and D. R. LaFosse, *Phys. Rev. C* **63**, 061304(R) (2001).
 [8] R. A. Bark, A. M. Baxter, A. P. Byrne, G. D. Dracoulis, T. Kibédi, T. R. McGoram, and S. M. Mullins, *Nucl. Phys. A* **691**, 577 (2001).
 [9] K. Starosta, C. J. Chiara, D. B. Fossan, T. Koike, T. T. S. Kuo, D. R. LaFosse, S. G. Rohozinski, Ch. Droste, T. Morek, and J. Srebrny, *Phys. Rev. C* **65**, 044328 (2002).
 [10] T. Koike, K. Starosta, C. J. Chiara, D. B. Fossan, and D. R. LaFosse, *Phys. Rev. C* **67**, 044319 (2003).
 [11] G. Rainovski *et al.*, *Phys. Rev. C* **68**, 024318 (2003).
 [12] G. Rainovski *et al.*, *J. Phys. G* **29**, 2763 (2003).
 [13] S. Zhu *et al.*, *Phys. Rev. Lett.* **91**, 132501 (2003).
 [14] H. C. Jain, S. Lakshmi, and P. K. Joshi, *AIP Conf. Proc.* **764**, 99 (2005).
 [15] J. Srebrny, E. Grodner, T. Morek, I. Zalewska, Ch. Droste, J. Mierzejewski, A. A. Pasternak, J. Kownacki, and J. Perkowski, *Acta Phys. Pol. B* **36**, 1063 (2005).
 [16] E. Grodner *et al.*, *Phys. Rev. Lett.* **97**, 172501 (2006).
 [17] C. Vaman, D. B. Fossan, T. Koike, K. Starosta, I. Y. Lee, and A. O. Macchiavelli, *Phys. Rev. Lett.* **92**, 032501 (2004).
 [18] P. Joshi *et al.*, *Phys. Lett. B* **595**, 135 (2004).
 [19] P. Joshi *et al.*, *Eur. Phys. J. A* **24**, 23 (2005).
 [20] J. A. Alcántara-Núñez *et al.*, *Phys. Rev. C* **69**, 024317 (2004).
 [21] J. Timár *et al.*, *Phys. Lett. B* **598**, 178 (2004).
 [22] J. Timár, C. Vaman, K. Starosta, D. B. Fossan, T. Koike, D. Sohler, I. Y. Lee, and A. O. Macchiavelli, *Phys. Rev. C* **73**, 011301(R) (2006).
 [23] D. Tonev, *et al.* *Phys. Rev. Lett.* **96**, 052501 (2006).
 [24] D. Tonev *et al.*, *Phys. Rev. C* **76**, 044313 (2007).
 [25] P. Olbratowski, J. Dobaczewski, and J. Dudek, *Phys. Rev. C* **73**, 054308 (2006).
 [26] S. Brant, D. Vretenar, and A. Ventura, *Phys. Rev. C* **69**, 017304 (2004).
 [27] C. M. Petrache, G. B. Hagemann, I. Hamamoto, and K. Starosta, *Phys. Rev. Lett.* **96**, 112502 (2006).
 [28] C. W. Beausang, L. Hildingsson, E. S. Paul, W. F. Piel Jr., N. Xu, and D. B. Fossan, *Phys. Rev. C* **36**, 1810 (1987).
 [29] K. Hauschild *et al.*, *Phys. Rev. C* **50**, 707 (1994).

- [30] M. N. Rao *et al.*, *Phys. Rev. C* **58**, 1367(R) (1998).
- [31] Gammasphere Proposal, LBNL-PUB-5202; I. Y. Lee, *Nucl. Phys. A* **520**, 361 (1990).
- [32] R. V. F. Janssens and F. S. Stephens, *Nucl. Phys. News* **6**, 9 (1996).
- [33] M. Devlin, L. G. Sobotka, D. G. Sarantites, and D. R. LaFosse, *Nucl. Instrum. Methods A* **383**, 506 (1996).
- [34] E. S. Paul *et al.*, *Phys. Rev. C*. (in press).
- [35] P. J. Nolan and J. F. Sharpey-Schafer, *Rep. Prog. Phys.* **42**, 1 (1979).
- [36] M. Cromaz, T. J. M. Symons, G. J. Lane, I. Y. Lee, and R. W. MacLeod, *Nucl. Instrum. Methods A* **462**, 519 (2001).
- [37] D. C. Radford, *Nucl. Instrum. Methods A* **361**, 297 (1995); **361**, 306 (1995); [<http://radware.phy.ornl.gov>].
- [38] K. Starosta, D. B. Fossan, T. Koike, C. Vaman, D. C. Radford, and C. J. Chiara, *Nucl. Instrum. Methods A* **515**, 771 (2003).
- [39] A. Krämer-Flecken, T. Morek, R. M. Lieder, W. Gast, G. Hebbinghaus, H. M. Jeger, and W. Urban, *Nucl. Instrum. Methods A* **275**, 333 (1989); K. S. Krane, R. M. Steffen, and R. M. Wheeler, *Nucl. Data Tables A* **11**, 351 (1973).
- [40] R. Arlt, G. Beyer, V. Fominykh, E. Herrmann, A. Jasinski, H. G. Ortlepp, H. Strusny, H. Tyrroff, and Z. Usmanova, *Acta Phys. Pol. B* **4**, 301 (1973).
- [41] Yu. V. Sergeenkov, *Nucl. Data Sheets* **71**, 557 (1994).
- [42] A. Gade, I. Wiedenhover, M. Luig, A. Gelberg, H. Meise, N. Pietralla, V. Werner, and P. von Brentano, *Nucl. Phys. A* **673**, 45 (2000).
- [43] S. P. Roberts, T. Ahn, K. Starosta, T. Koike, C. J. Chiara, and C. Vaman, *Phys. Rev. C* **67**, 057301 (2003).
- [44] T. Kibédi, T. W. Burrows, M. B. Trzhaskovskaya, P. M. Davidson, and C. W. Nestor Jr., *Nucl. Instrum. Methods A* **589**, 202 (2008).
- [45] A. A. Sonzogni, *Nucl. Data Sheets* **103**, 1 (2004).
- [46] E. S. Paul *et al.*, *Nucl. Phys. A* **690**, 341 (2001).
- [47] R. Ma, E. S. Paul, C. W. Beausang, S. Shi, N. Xu, and D. B. Fossan, *Phys. Rev. C* **36**, 2322 (1987).
- [48] E. S. Paul *et al.*, *Nucl. Phys. A* **619**, 177 (1997).
- [49] F. Dönau and S. Frauendorf, in *Proceedings of the Conference on High Angular Momentum Properties of Nuclei*, edited by N. R. Johnson (Harwood Academic, New York, 1983), p. 143; F. Dönau, *Nucl. Phys. A* **471**, 469 (1987).
- [50] D. C. Radford *et al.*, *Nucl. Phys. A* **545**, 665 (1992).
- [51] S. Törmänen *et al.*, *Nucl. Phys. A* **572**, 417 (1994).
- [52] A. M. Bizetti-Sona *et al.*, *Z. Phys. A* **335**, 365 (1990); P. Raghavan, *At. Data Nucl. Data Tables* **42**, 189 (1989).
- [53] R. Bengtsson and S. Frauendorf, *Nucl. Phys. A* **327**, 139 (1979).
- [54] W. Nazarewicz, G. A. Leander, and J. Dudek, *Nucl. Phys. A* **467**, 437 (1987).
- [55] W. Nazarewicz, R. Wyss, and A. Johnson, *Nucl. Phys. A* **503**, 285 (1989).
- [56] R. Wyss, J. Nyberg, A. Johnson, R. Bengtsson, and W. Nazarewicz, *Phys. Lett. B* **215**, 211 (1988).
- [57] L. L. Riedinger *et al.*, *Acta Phys. Pol. B* **32**, 2613 (2001).
- [58] G. Andersson *et al.*, *Nucl. Phys. A* **268**, 205 (1976).
- [59] C. J. Gallagher Jr. and S. A. Moszkowski, *Phys. Rev.* **111**, 1282 (1958).
- [60] L. Hildingsson, C. W. Beausang, D. B. Fossan, and W. F. Piel Jr., *Phys. Rev. C* **37**, 985 (1988).